4. ASSESSMENT OF LANDSLIDE AFFECTED AREAS USING SATELLITE DIGITAL DATA

4-1 METHODS OF ANALYSIS

In this chapter, the potential of multitemporal Landsat Thematic Mapper (TM) data to identify landslide-affected area was examined. This was done by determining the changes in spectral characteristics exhibited by land cover, in response to disturbances in visible, infrared and mid infrared parts of the spectrum. The digital images obtained prior to and following a disaster were analyzed using five different kinds of change detection techniques. The change detection techniques applied are 1) spectral image differencing, 2) vegetation index image differencing, 3) tasseled cap transformation image differencing, 4) spectral change vector analysis, and 5) principal component analysis. Different change detection techniques were then compared for their applicability in the assessment of affected areas associated with landsliding.

4-1-1 The Remotely Sensed Satellite Digital Data

Two Landsat TM images dated 20 December 1990 and 29 December 1993 of Path 144, Row 041 were used for the analysis. The 1990 image characterizes the pre-disaster condition, and that of 1993 characterizes the post-disaster condition. Since land use had not changed appreciably in the study area between 1990 and 1993, it was expected that the spectral changes exhibited in 1993 should reflect the effect of landsliding. When the change detection analysis is based on data acquired in the same season, immediately prior to, and following a disturbance, spectral changes should be related to disturbance change with a reasonably high degree of certainty. Otherwise, spectral changes associated with a specific disturbance may be confounded with land-use change, annual phenological differences, climate, and other factors that differ between the pre- and post-disturbance imagery. Figure 4-1 is a full scene of Path 144, Row 041, bulk rectified TM data of 29 December 1993, which was one of the two pieces of data used in this study. The processes of change detection techniques employed can be broadly categorized into three phases as pre-processing of the data, selection of change detection algorithms and analysis, and thresholding and accuracy assessment. Figure 4-2 is the flow diagram of the change detection technique stages.

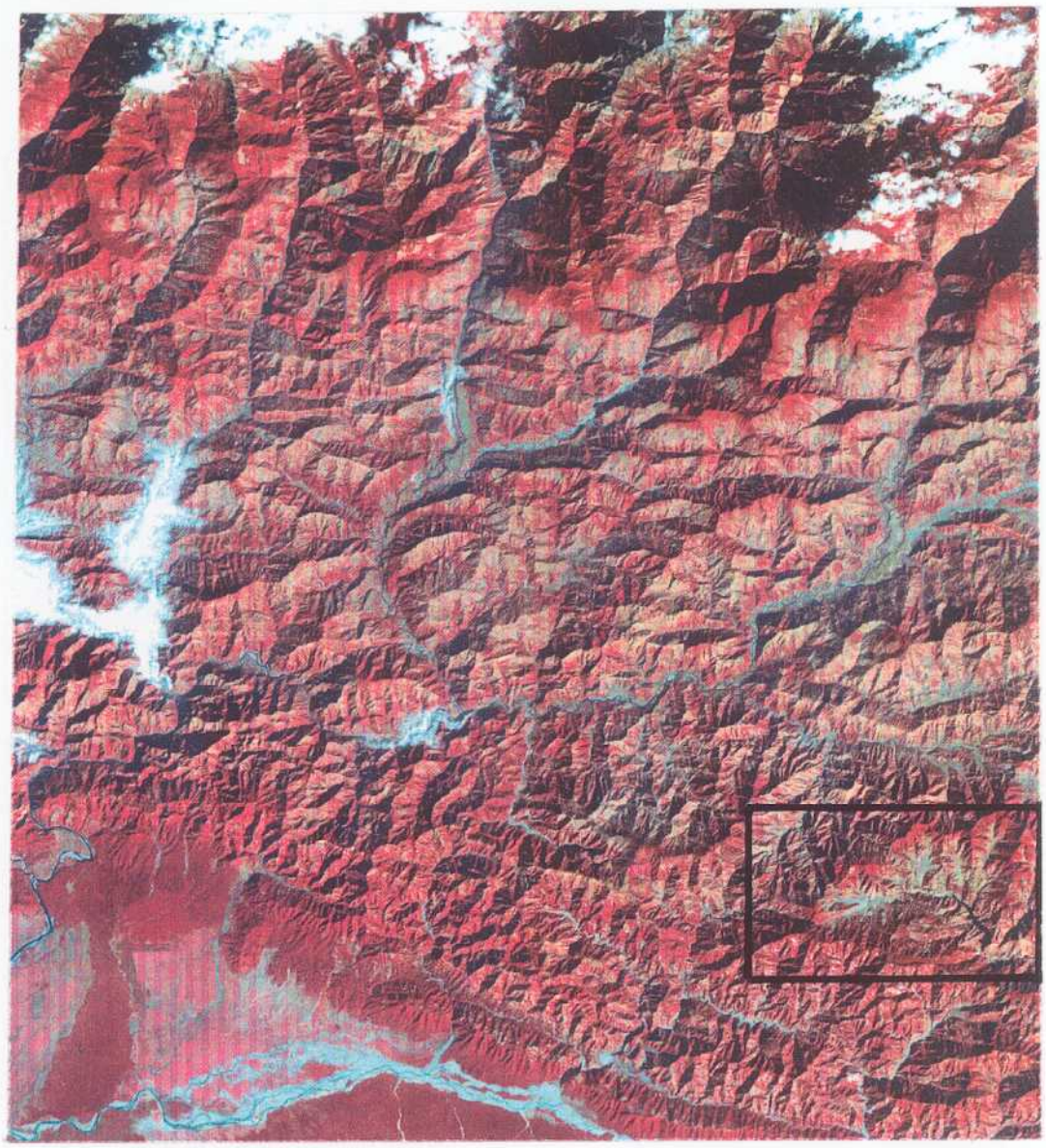

Figure 4-1 Landsat thematic mapper image (full scene) of path-141 row-041 of 29 December 1993 (bulk rectified) with the band 4, 3 and 2 displayed in red, green and blue, respectively. The scene covers 185 km x 172 km. Kulekhani watershed is bounded by a rectangle in the fourth quadrant (bottom right).

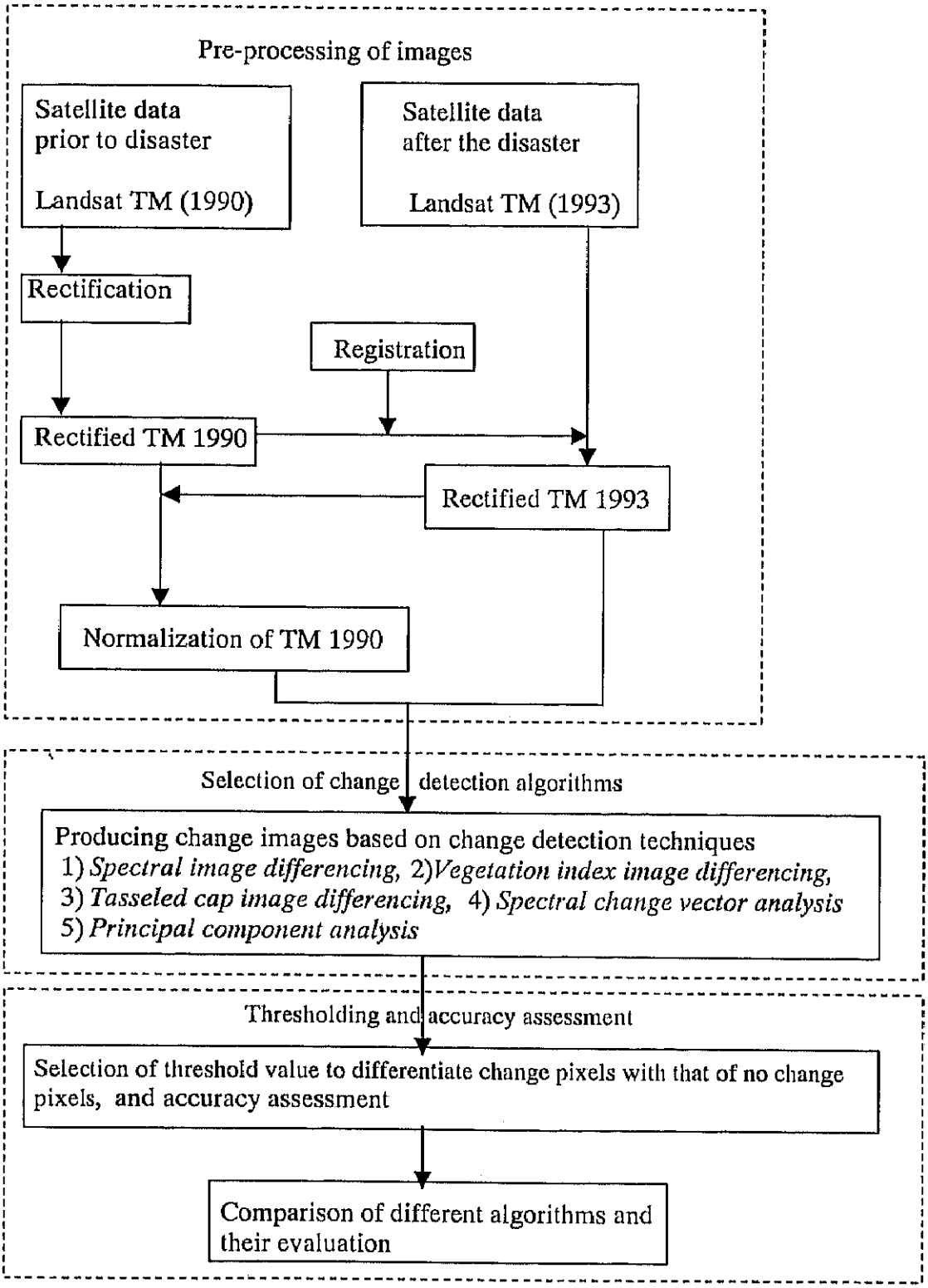

Figure 4-2 Flow diagram of change detection processes for the assessment of landslide affected areas using satellite digital data.

4-1-2 Pre-processing of TM Data

When a sensor on a satellite records the image data, it may contain errors in both geometry and the measured brightness values of the pixel. Errors in image geometry are caused due to 1) rotation of the earth during image acquisition, 2) wide field of view of sensors, 3) curvature of the earth, 4) type of sensor, 5) variation in platform altitude and velocity, and 6) panoramic effects related to image geometry. The geometric distortions present in the images need to be corrected when data taken at different times are to be compared, or when GIS operations such as overlay are to be performed.

In addition, a problem associated with using multitemporal remotely sensed data for change detection is that the data are usually captured with varying sun angle, atmospheric, and soil moisture conditions. Ideally, the multiple dates of remotely sensed data should be "normalized" so that these effects can be minimized or eliminated (Eckhardt *et al.*, 1990; Hall *et al.*, 1991).

4-1-2.1 Geometric rectification

There are two techniques to correct geometric distortions present in a digital image. In the first method, the nature and magnitude of the distortion is modeled mathematically by quantifying the causes of distortions. The method requires characterization of the distortions precisely. The second method is to define a mathematical relationship between the addresses of image pixels to corresponding ground coordinates via maps or other coordinate information. This is the method applied in this study. In this method, it is required to identify clearly identifiable features on the image and corresponding ones on maps. These well defined points both in the image and maps are called control points.

Thirty four ground control points (GCPs) digitized from the topographic map of scale 1:25000 were used to rectify the 20 December 1990 Landsat TM image to a Universal Transverse Mercator (UTM) map projection (root mean square error: RMSE = 0.46 pixel / 14 m). The RMSE in the X-direction and Y-direction were respectively 0.30 and 0.35 pixel. The 1993 image was registered using 50 GCPs obtained from the rectified 1990 image (RMSE = 0.31 pixel / 9 m). The RMSE in the X-direction and Y-direction were respectively 0.19 and 0.24 pixel. The RMSE were considered acceptable for carrying out the pixel to pixel change detection analysis. The images were

resampled to a 30 m pixel size using the nearest neighbor resampling technique to retain radiometric integrity (Jensen, 1996). Figure 4-3 is the geometrically rectified TM images of 1990 and 1993 with the boundary of the study area overlaid.

4-1-2.2 Image normalization

The ability to use remotely sensed data to change detection is based upon the fact that a relationship between data captured by a sensor and actual surface conditions do exist. However, factors such as sun angle, Earth/sun distance detector calibration, differences between the various sensor systems, atmospheric condition, and sun/ target/ sensor (phase angle) geometry will also affect pixel brightness value (BV) between dates. Differences in the direct-beam solar radiation due to variation in sun angle and Earth/sun distance can be calculated accurately, as can variation in pixel BVs due to detector calibration differences between sensor systems. However, removal of atmospheric and phase angle effects require information about the gaseous and aerosol composition of the atmosphere and the bi-directional reflectance characteristics of elements within the scene (Eckhardt *et al.*, 1990). Because the atmospheric and bi-directional information is usually not available, an empirical scene normalization approach was used to match the detector calibration, astronomic, atmospheric, and phase angle conditions present in a reference scene.

The 1993 TM scene was selected as the reference scene to which the 1990 scene was normalized, because large-scale aerial photographs were available for the date close to the 1993 TM data. The image normalization was achieved by applying regression equations to the 1990 imagery which predicted what a given BV would be if it had been acquired under the same conditions as the 1993 reference scene. For this, operation pixel clusters of "normalization targets" were extracted from wet (water; reservoir) and dry (rock outcrops and grassland) areas in both the 1993 and 1990 images. Normalization targets were assumed to be the constant reflectors, so any changes in their brightness values were attributed to astronomic, atmospheric, and phase angle differences. In this study, normalization targets consist of three points in the reservoir area, three points from rock outcrops, and three points from the grassland. These points were first located on the available aerial photographs. They were then examined in both images using a display device for their similarity in natural color

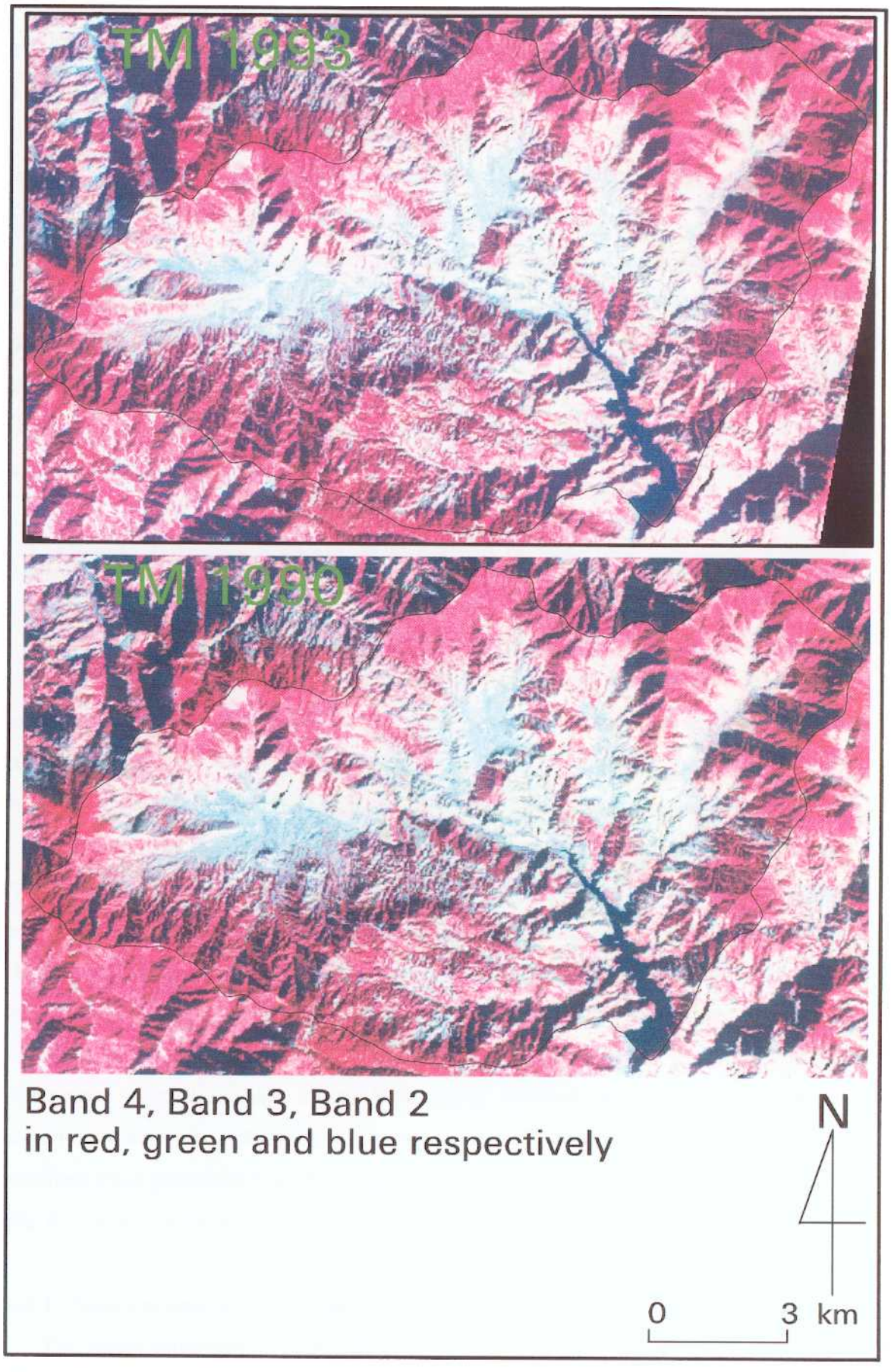

Figure 4-3 Post- and pre-disaster Landsat TM images (rectified) used for the study.

composites. Finally, the points were then confirmed from the field survey using GPS. The pixel values for these points from each band were plotted against each other to verify the linear relationships between the data of both images. The linear relationships existed. Then the regression equation was derived for the relationship for each band (Figure 4-4). The coefficients and intercept of the equation were used to obtain normalized 1990 TM image. Each regression model contained an additive component that corrected for the difference in atmospheric path radiance between dates, and a multiplicative term that corrected for the difference in detector calibration, sun angle, Earth/sun distance, atmospheric attenuation, and phase angle between dates. Once these variations in the multiple date images were removed, changes in BV could be related to changes in surface conditions.

4-1-3 Change Detection Techniques Examined in Detecting Landslide Affected Areas

The identification of landslide affected areas using multitemporal data is based on the assumption that, the disturbances such as landsliding cause abrupt changes in spectral characteristics exhibited by land covers in the visible, infra red and mid infrared part of the spectrum. The average brightness value (BV) extracted for different areas affected by landsliding from the images of 1993 and 1990 are shown on Figure 4-5 (A-L). The location of these areas were measured (at least 100 m wide) in the field with GPS. The measured location values were brought into ARC/INFO and rasterized before overlaying with the 1990 and 1993 images. Table 4-1 summarizes the preliminary understanding (based on Figure 4-5) on the characteristics of six different bands for detecting different type of changes, as landslides or sediment deposition. With this information in mind, five different change detection methods such as spectral image differencing, vegetation index image differencing, tasseled cap differencing, spectral change vector analysis, and principal component analysis were employed. Altogether 11 algorithms were generated from these five methods. These are subsequently discussed. Table 4-2 shows the details on the change detection techniques applied in this study.

4-1-3.1 Spectral image differencing

The image differencing technique was performed by subtracting the BV

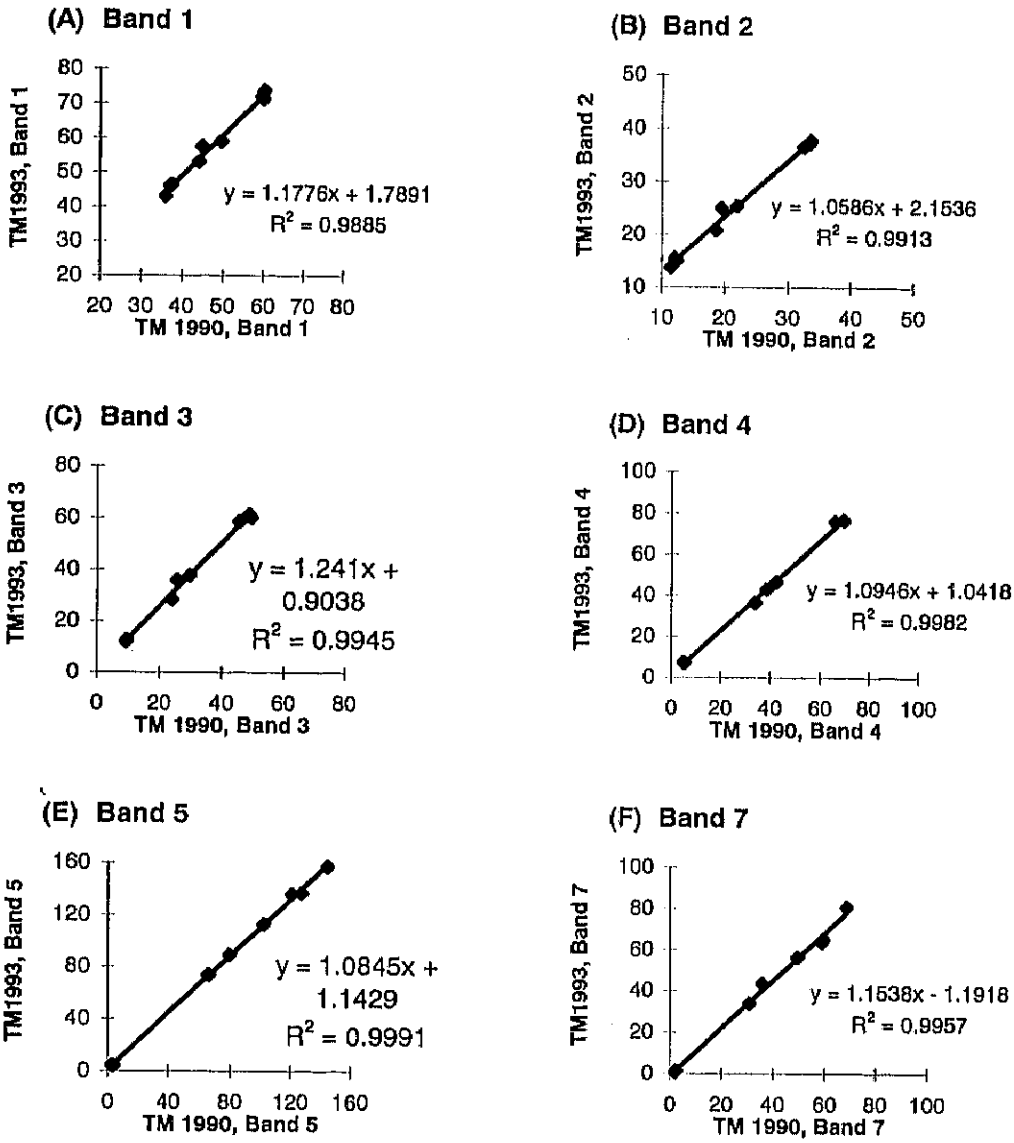

Figure 4-4 (A-F) Relationships between the same wet and dry regions found in both 20 December 1990 and 29 December 1993 in TM bands 1-7 (excluding band 6). The regression equations are used to normalize radiometric characteristics of the 1990 TM data.

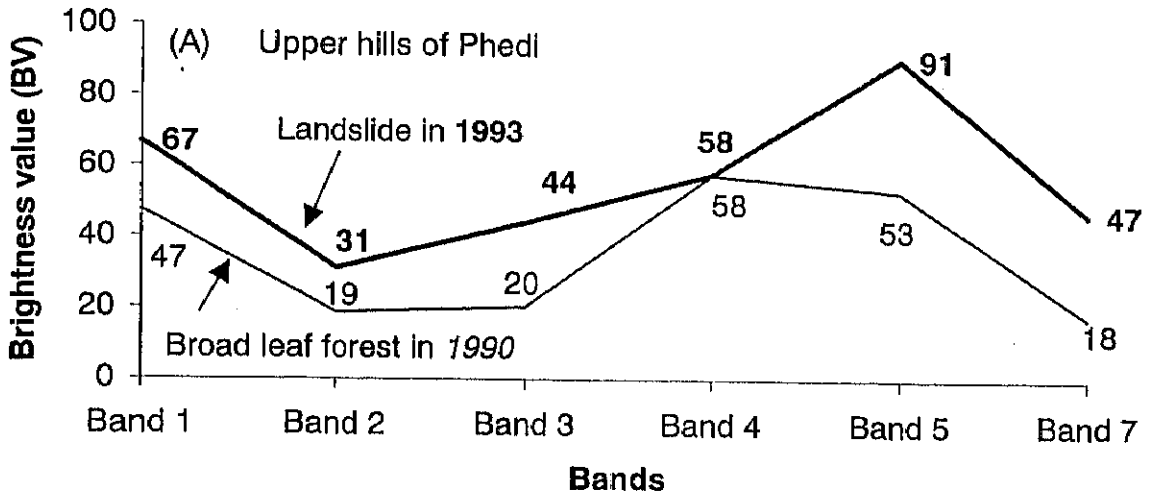

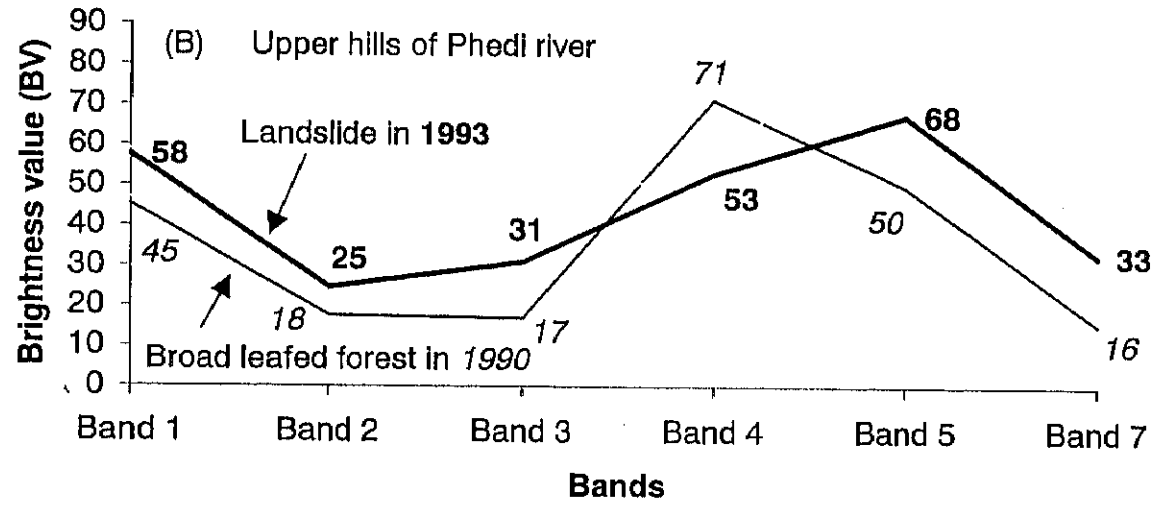

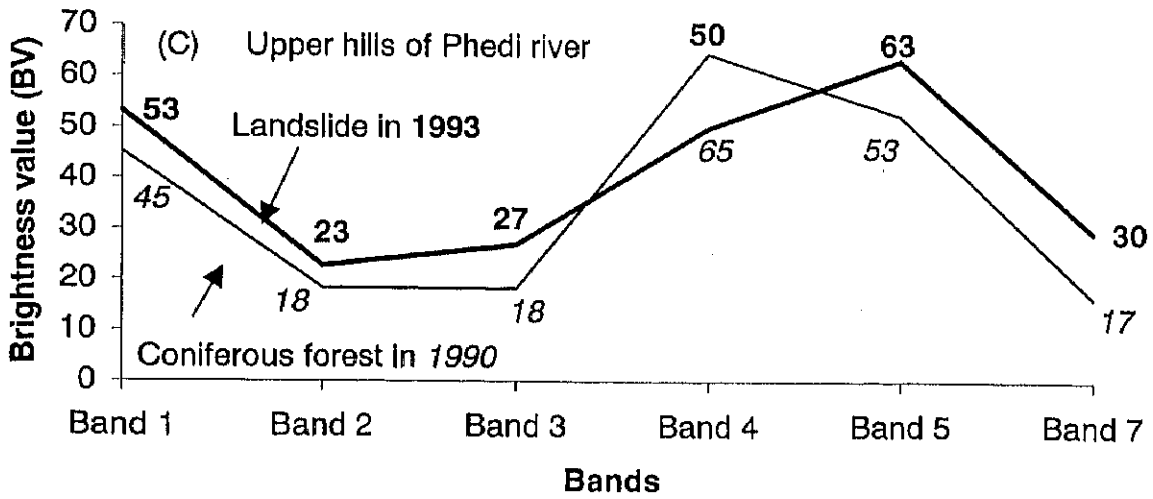

Figure 4-5 (A-L) Change in brightness value for areas affected by landsliding extracted from TM 1993 and TM 1990. The values depicted are an average of 9 pixels (3 x 3 window) in most of cases excluding for few landslides which show an average of 4 pixels. For place names see Figure 2-1.

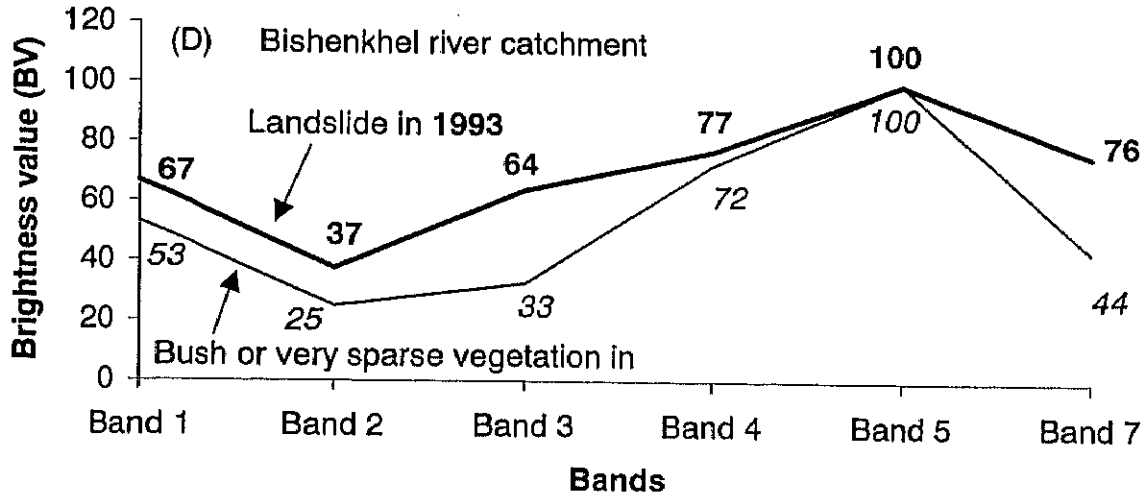

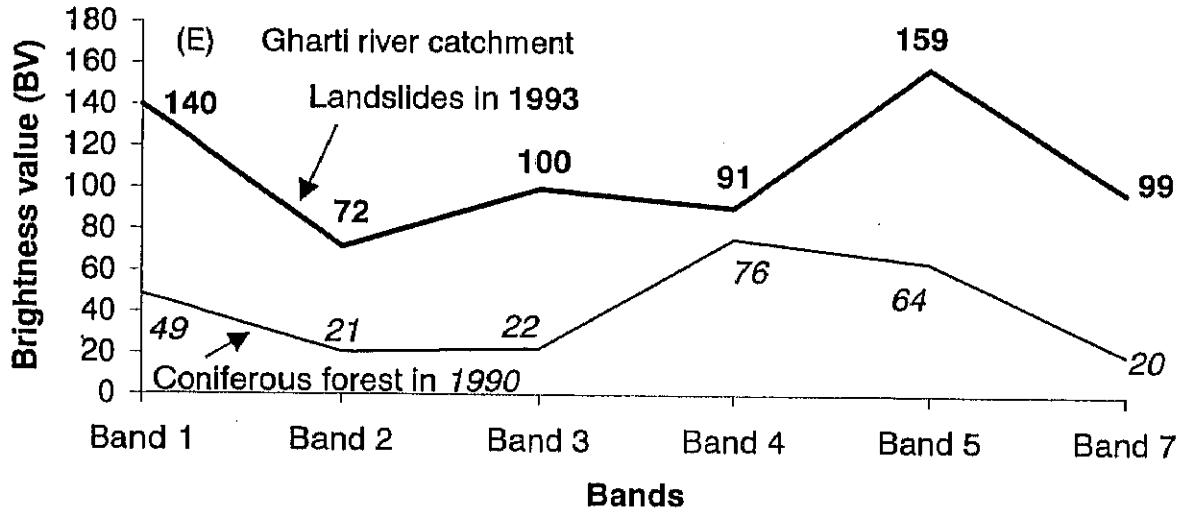

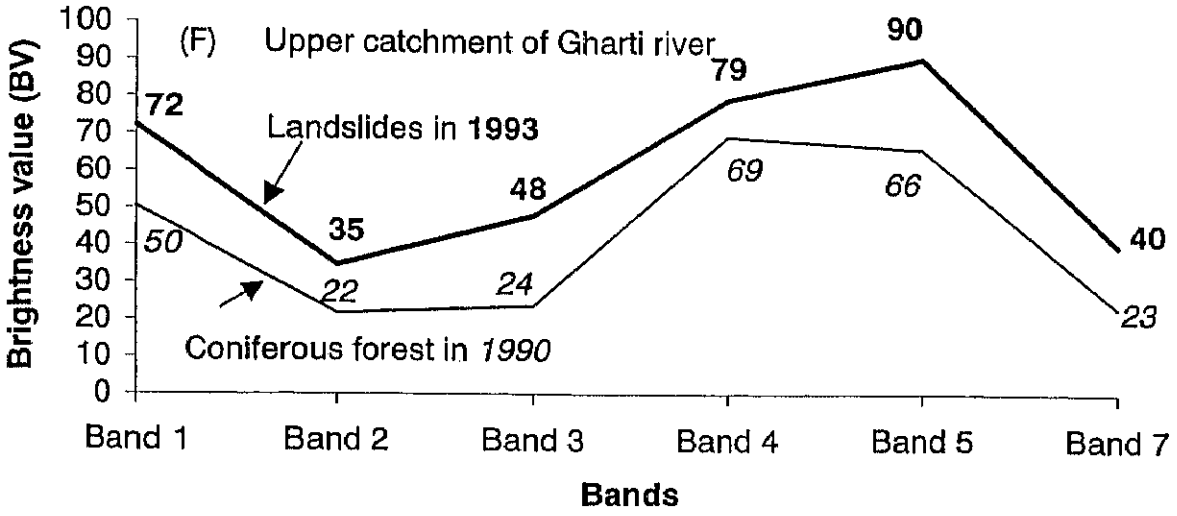

Figure 4-5 (continued).

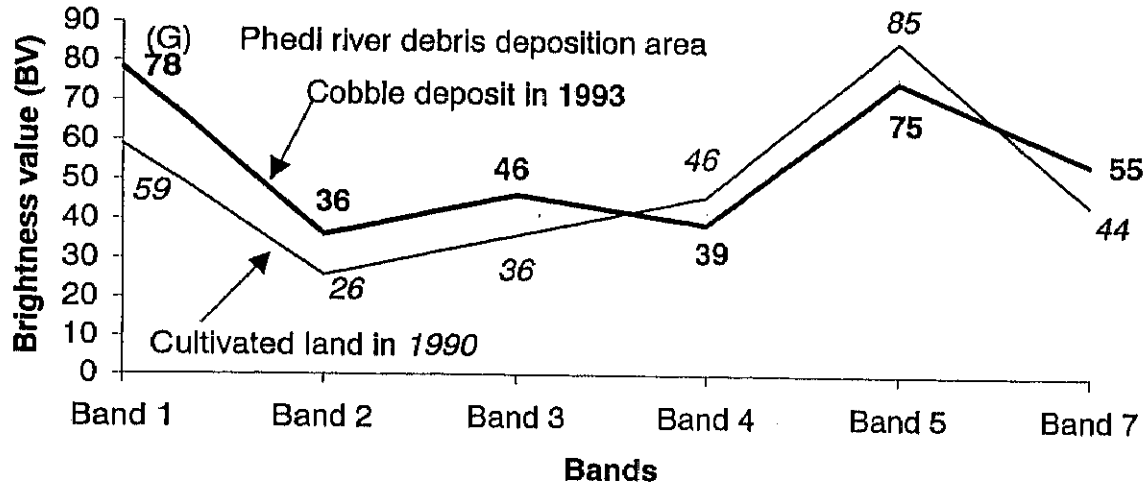

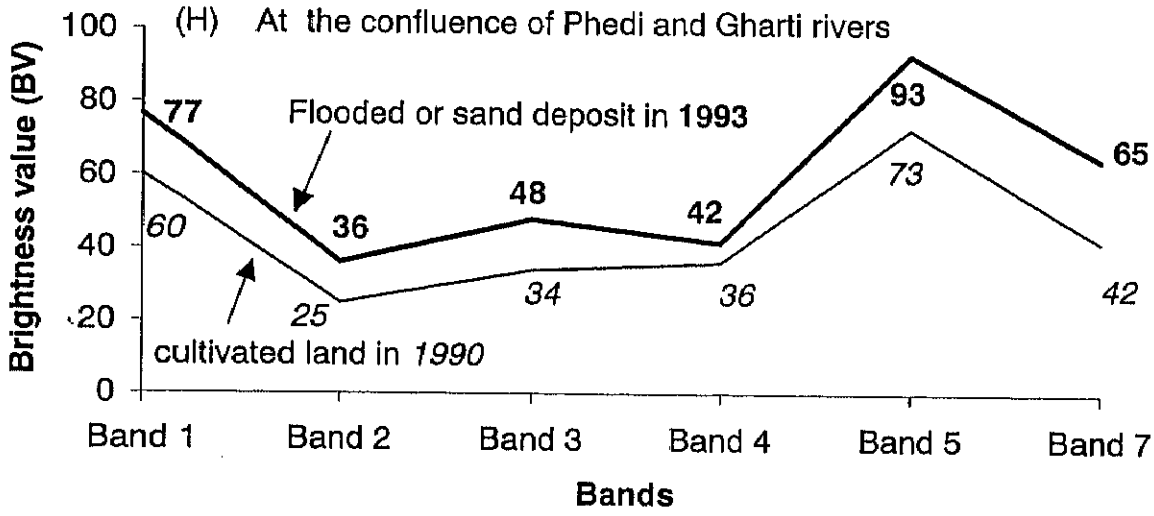

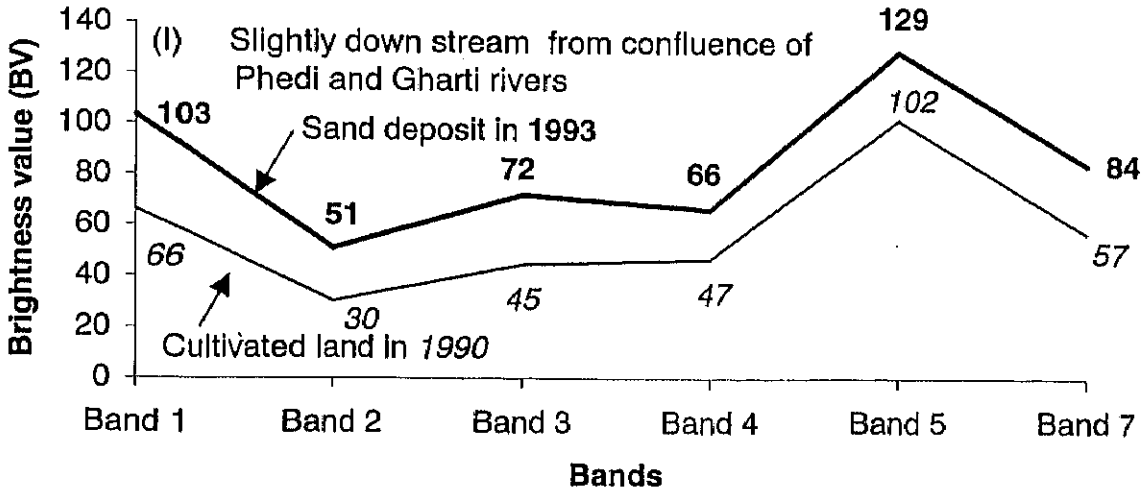

Figure 4-5 (Continued).

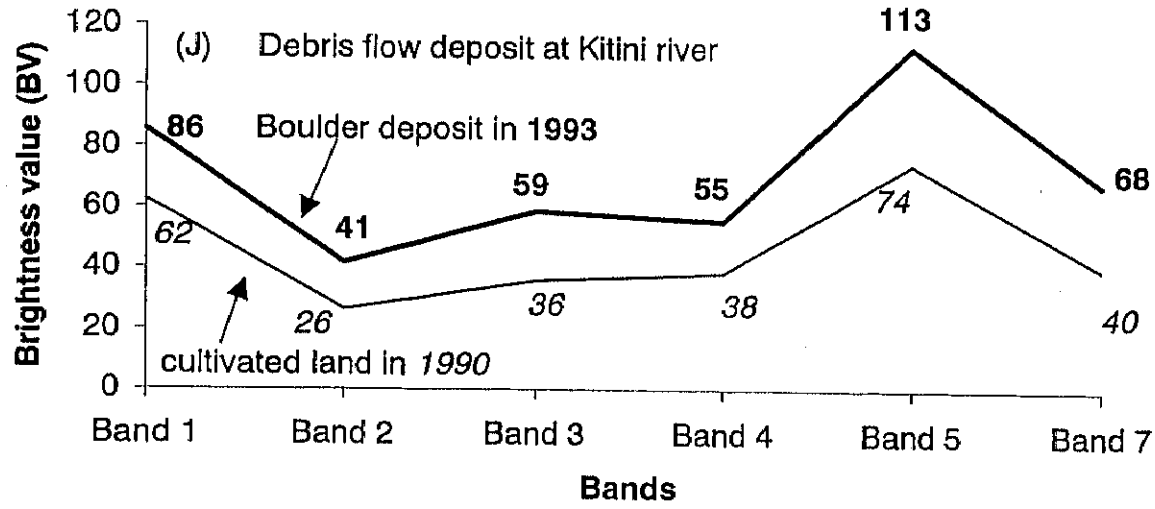

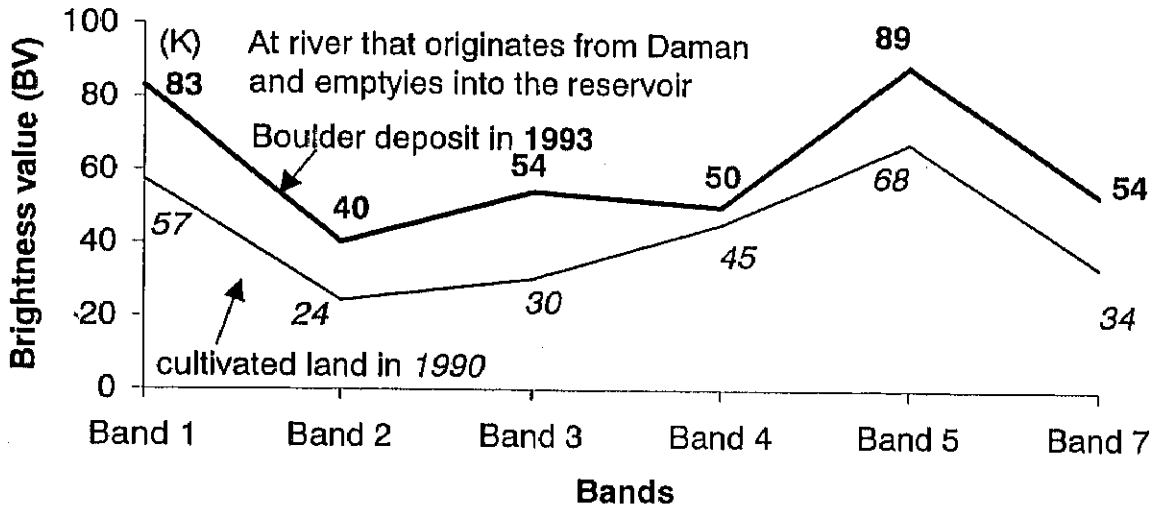

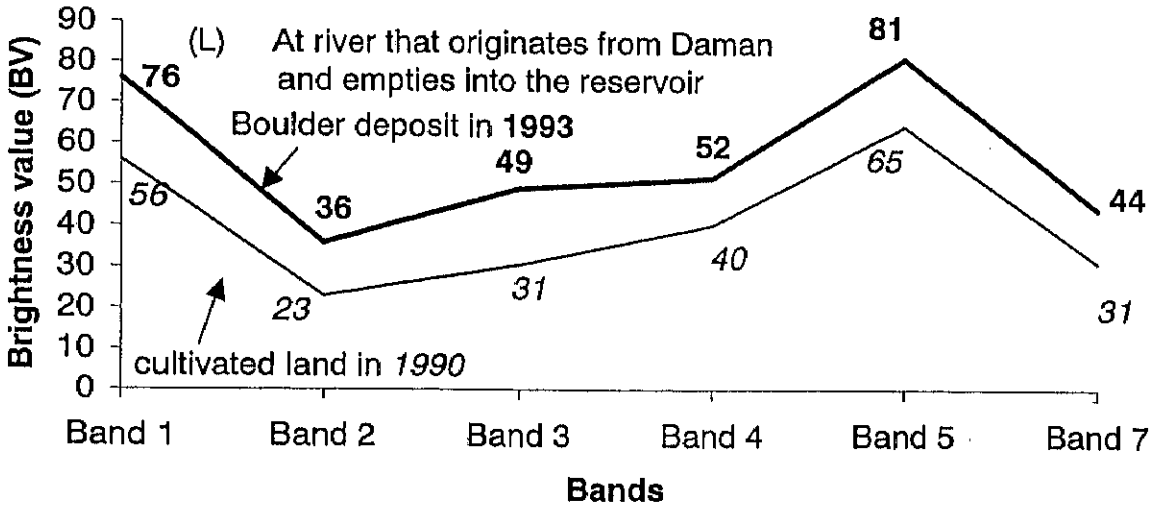

Figure 4-5 (Continued).

Table 4-1 Preliminary understanding on the characteristics of six different bands for detecting different types of landslide affected areas.

Bands	Landslides	Sediment deposition areas		
		Sand deposit	Cobble deposit	Boulder deposit
Band 1	increase in BV	increase in BV	increase in BV	increase in BV
Band 2	increase in BV	increase in BV	increase in BV	increase in BV
Band 3	increase in BV	increase in BV	increase in BV	increase in BV
Band 4	increase as well as decrease in BV	increase in BV	decrease in BV	increase in BV
Band 5	increase as well as decrease in BV	increase in BV	decrease in BV	increase in BV
Band 7	increase in BV	increase in BV	increase in BV	increase in BV

BV: Brightness value

Table 4-2 Change detection techniques employed in the study.

No.	Change Detection Techniques	Different algorithms within the change detection techniques	Total number of algorithms in each technique
1.	Spectral image differencing	1. Band 1	4
		2. Band 2	
		3. Band 3	
		4. Band 7	
2.	Vegetation index image differencing	1. Difference vegetation index image differencing	3
		2. Ratio vegetation index image differencing	
		3. Normalized difference vegetation index (NDVI) image differencing	
3	Tassalled cap transformation image differencing	1. Tasselled cap brightness function image differencing	1
4	Spectral change vector analysis	1. Band 1, band 2, and band 3 (sector code 8)	2
		2. Band 3 and band 4 (sector code 3)	
5	Principal component analysis	1. Band 1, band 2, and band 3	1
Total			11

(brightness value) of spatially registered TM images of 1990 to 1993, pixel by pixel in order to produce the change image which represented the change between the two times. Spectral image differencing was performed on the four bands (band 1: blue, band 2: green, band 3: red, and band 7: mid infrared). The selection of these bands was guided by their clear responses in the areas affected by landslide disturbances (see Figure 4-5). All these bands show clear increase in the BV in the affected areas.

The subtraction (differencing) produces an image data set where positive and negative values represent areas of change and values close to zero indicate areas that remain relatively unchanged. In an 8 bit analysis with pixel values ranging from 0 to 255 (256 levels), the potential range of difference values is –255 to 255. The range of the values in difference images were checked and transformed into positive values by adding the median value (127) to the original value resulting from the subtraction. For the pixel located at row i and column j, the difference in the brightness value (DBV^k_{ij}) for band k between the two dates can be mathematically written as;

$$DBV^k_{ij} = BV^k_{ij}(t_2) - BV^k_{ij}(t_1) + C \quad \text{----------(2)}$$

Where, BV = Brightness value, t_2 = second date (in this case 1993), t_1 = first date (in this case 1990), C = constant (taken as 127)

Figure 4-6 (A-D) show the smoothed histogram of four change images. The histograms show normal or nearly normal distribution in all cases. The mean, standard deviation, median, and mode values for each histogram are also shown. Values near the mean indicate they have similar spectral values on both dates, and therefore have experienced no disturbances. As values increase or decrease from the mean, greater change is presumed to have occurred between the dates. For TM bands 1, 2, 3 and 7, the values that are less than or close to mean (i.e. represented by the left side tail of the histogram) indicate areas where spectral values decreased in 1993 or remained relatively unchanged. These are the pixels, which are considered not affected by disturbances, because these pixels rather indicate the annual ephemeral changes in the land cover in which I was not interested. Hence, values greater than the mean, representing areas that exhibit an increase in brightness value (i.e. represented by the right side tail of the histogram) were considered as affected by landslides.

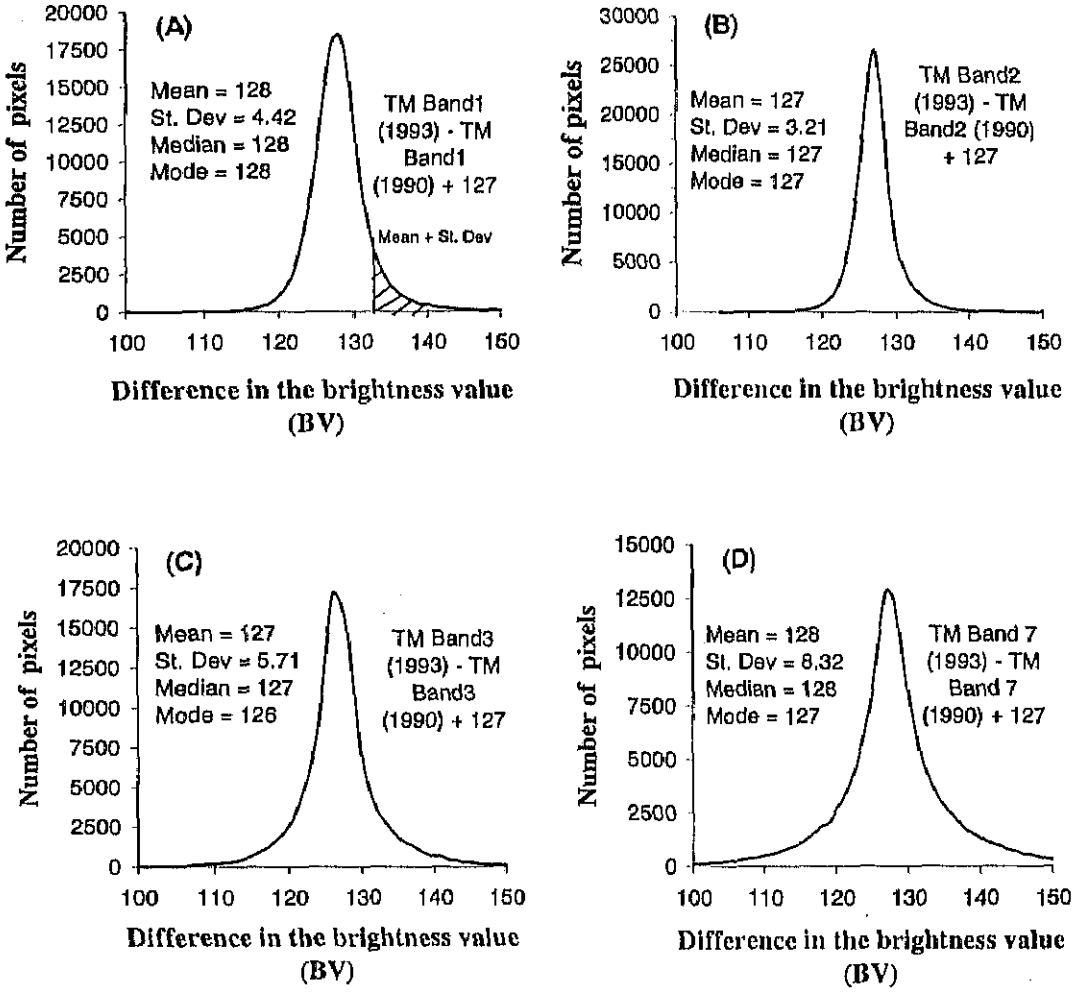

Figure 4-6 (A-D) Histograms of change images for spectral image differencing change detection method. Bands and statistics are shown.

The question in all change images was then where to place the threshold boundaries between change and no-change pixels displayed in the histogram of the change image. It is called thresholding and is a most critical element in change detection analysis. Considering the importance of the topic, thresholding and accuracy assessment are discussed below in detail.

Thresholding and accuracy assessment

Frequently the standard deviation from the mean is established as the threshold value, which has been usually found suitable (Jensen, 1996). However, in this study two steps were carried out to determine the threshold value. The following discussion illustrates the method of determination of the optimal threshold value employed. The histograms of the four change image sets were examined, and the mean and the standard deviation for each data set were calculated (see Figure 4-6). The threshold values, with which to separate the change pixels from the no change pixels were examined in the following way. In this procedure I took only the right side tail of the histogram for the reasons explained in the last section. I added the value of the standard deviation x N to the mean, with the starting value of N = 0.25 and the increment of 0.25 until N = 3.0. The threshold images produced are binary images in which a value of 0.0 or 1.0 represents no change or change, respectively.

In the first step, a range of threshold values depicting the "realistic amount of change" (Jensen, 1996) was selected based on the familiarity of the study area. Three surveys had been carried out between 1997 to 1999 and at least a month had been spent in the study area each time for this purpose and others. Then in the second step, the change images produced at each selected ranges of threshold were verified with the reference sample data. Error matrices were produced and analyzed for accuracy assessment for the ranges selected to determine the optimal threshold. Two accuracies, "overall accuracy" and "Khat" (kappa coefficient of agreement) were used. The producer's accuracy, which measures the error of omission and the user's accuracy that measures error of comission were also calculated.

The reference data for the accuracy assessment included randomly sampled areas of no change and change sites. The location of these areas were measured (at least 100 m wide with the exception of few landslides) in the field with GPS. The measured

location values were brought into ARC/INFO and rasterized before overlaying with the change images produced at ranges of threshold values. The reference data consisted of 1,468 pixels from the areas of no change, and 1,075 pixels from the areas affected by landsliding. Among 1,075 change pixels, 388 pixels represented landslides (slope failures) pixels, and the rest represented the sediment deposited areas located in the alluvial fan and river terraces. The change in spectral bands 1, 2, 3 and 7 were considered to depict both landslides and sediment deposited areas in terms of overall affected areas and the accuracy assessment was carried out with 1,468 no change pixels and 1,075 change pixels. The various accuracies used for the thresholding are described below. Table 4-3 shows the example of calculation of various accuracies from the error matrix for the change image produced, using band 1 at threshold when N equals 1.

The overall accuracy is the total number of correctly classified samples (diagonal cells of the matrix) divided by the total number of samples. It is 0.87 in Table 4-3. It measures the accuracy of the entire image without any indication of the accuracy of individual categories. Overall accuracy has a tendency to be biased toward the category with a larger number of samples (Nelson 1983; Singh 1986). It is for this reason, that the Khat accuracy was given importance in this study as it uses all the elements of the matrix. The Khat, also known as kappa coefficient of agreement, was originally developed by Cohen (Bishop et al., 1975) and is calculated as shown below.

$$k = \frac{\sum_{i=1}^{r} x_{ii} - \sum_{i=1}^{r} (x_{i+} \times x_{+i})}{N^2 - \sum_{i=1}^{r} (x_{i+} * x_{+i})} \qquad \text{----------(3)}$$

where, r is the number of rows in the matrix, x_{ii} is the number of observations in row i and column i (ith diagonal element), x_{i+} and x_{+i} are the marginal totals of row i and column i respectively, N is the total number of observations. The Khat takes into account the degree of agreement expected by chance by using all elements of the matrix and not just the main diagonal to its calculation. It represents the proportion of agreement obtained after removing the proportion of chance agreement. The Khat value in Table 4-3 is 0.726.

Table 4-3 Generation of error matrix and calculation of different accuracy measures in order to set a threshold value. An example of Band 1 change image; threshold value = mean + standard deviation (i.e. N = + 1).

		Reference data		
		No Change	Change	Total
Classified data	No Change	1411	274	1685
	Change	57	801	858
	Total	1468	1075	2543

Overall accuracy	(1411 + 801) / 2543 = 0.870
Khat	0.726 (For calculation see text)

Producer's accuracy		User's accuracy	
No Change	1411/1468 = 0.961	No Change	1411/1685 = 0.837
Change	801/1075 = 0.745	Change	801/858 = 0.934

The producer's accuracy is the number of correctly classified samples of a particular category divided by the total number of reference samples for that category. In Table 4-3, it is 0.745 (801/1075) and measures the error of omission. The user's accuracy is an alternative measure for individual category accuracy. It is a measure of correctly classified samples of a particular category divided by the total number of classified samples for that category. In Table 4-3, it is 0.934 (801/858) and measures the error of comission. Producer's accuracy refers to how well the producer of a map can delineate the areas of change and no change. For example, if the producer of a map is standing on some change area in the field, the producer's accuracy for change class refers to the probability of that area (on which he is standing) being identified as change on the map. The user's accuracy is the accuracy in which the user is interested. For example, if the user chooses one of the change areas from the map, the user's accuracy represents the probability that the area actually changes in the field.

4-1-3.2 Vegetation index image differencing

Landsat TM Band 3 and 4 are well suited for monitoring green vegetation. The 0.63 to 0.69 μm region (band 3) is centered on the chlorophyll absorption wavelengths of a green canopy. The 0.8 to 1.1 μm of the infrared region (where band 4 of TM falls) is highly reflected by vegetation due to the internal structure of the leaf (Tucker and Maxwell, 1976). Hence the development of vegetation indices from brightness values is based on the differential absorption, transmittance, and reflectance of the energy by the vegetation in the red (band 3) and infrared (band 4). It has been shown over the years that the ratio of near infrared MSS band 4 and red MSS band 2 is significantly correlated with the amount of green leaf biomass (Tucker, 1979; Nelson, 1983; Anderson and Hanson, 1992). The same is true with the bands 4 and 3 of TM data.

Numerous vegetation indices have been formulated to make use of the differences of red and infrared bands. The use of TM data in the derivation of different vegetation indices have been discussed in detail by Richardson and Everitt (1992), and Lyon *et al.* (1998). Basic techniques include the subtraction of the near infrared band and red band, the division of near infrared by the red band, and the combination of both in such a way so as to seek to normalize the response such as normalized difference vegetation Index (NDVI). I use in this study three types of vegetation indices image differencing, which

are called difference vegetation index (Band 4 - Band 3) image differencing, ratio vegetation index (Band 4 / Band 3) image differencing, and normalized difference vegetation index [NDVI: (Band 4 - Band 3) / (Band 4 + Band 3)] image differencing. Each of the three vegetation index image produced for 1990 was subtracted from that of 1993 to produce three change images: the change in difference vegetation index, the change in ratio vegetation index, and the change in NDVI.

The vegetation index change images are the images, showing changes in remote sensing measurements directly related to green biomass between 1990 and 1993. When landslide or debris-flow occurs in vegetated areas, it is expected that vegetation (green biomass) will be damaged or disturbed. With this, I hypothesized that the decrease in vegetation should imply the disturbance in vegetation due to landsliding. Hence, pixels which showed values smaller than the mean or close to the mean (the left side tail of the histogram) were considered to detect vegetation responses to disturbances (Figure 4-7 A-C). Pixels whose values are greater than or close to the mean (the right side tail of the histogram) indicate areas where vegetation indices increased in 1993 or remained relatively unchanged. These pixels rather indicate the annual ephemeral changes in the vegetation which was of no concern in this study, hence were not considered for further analysis. In Figure 4-7 (A-C) a factor should be noted concerning the characteristics of this data transformation. The change image produced from the difference vegetation index, is an 8-bit image in which a median value of 127 was added. However, the ratio and the normalized vegetation index differencing images are real, continuous images in which an arbitrary constant of 5 and 2 were added respectively, in order to produce a non-negative image.

Thresholding and accuracy assessment

The threshold value that separated the pixels of change from those of no change determined following two steps in the same way as explained in the preceding section. Vegetation indices were expected to show the vegetation responses to disturbances. The reference data in non-vegetated areas for accuracy assessment in this case were alluvial fan or river terraces, where sediment deposition had been observed. Hence, the accuracy assessment was carried out using 1,468 no change pixels and 388 landslide pixels only.

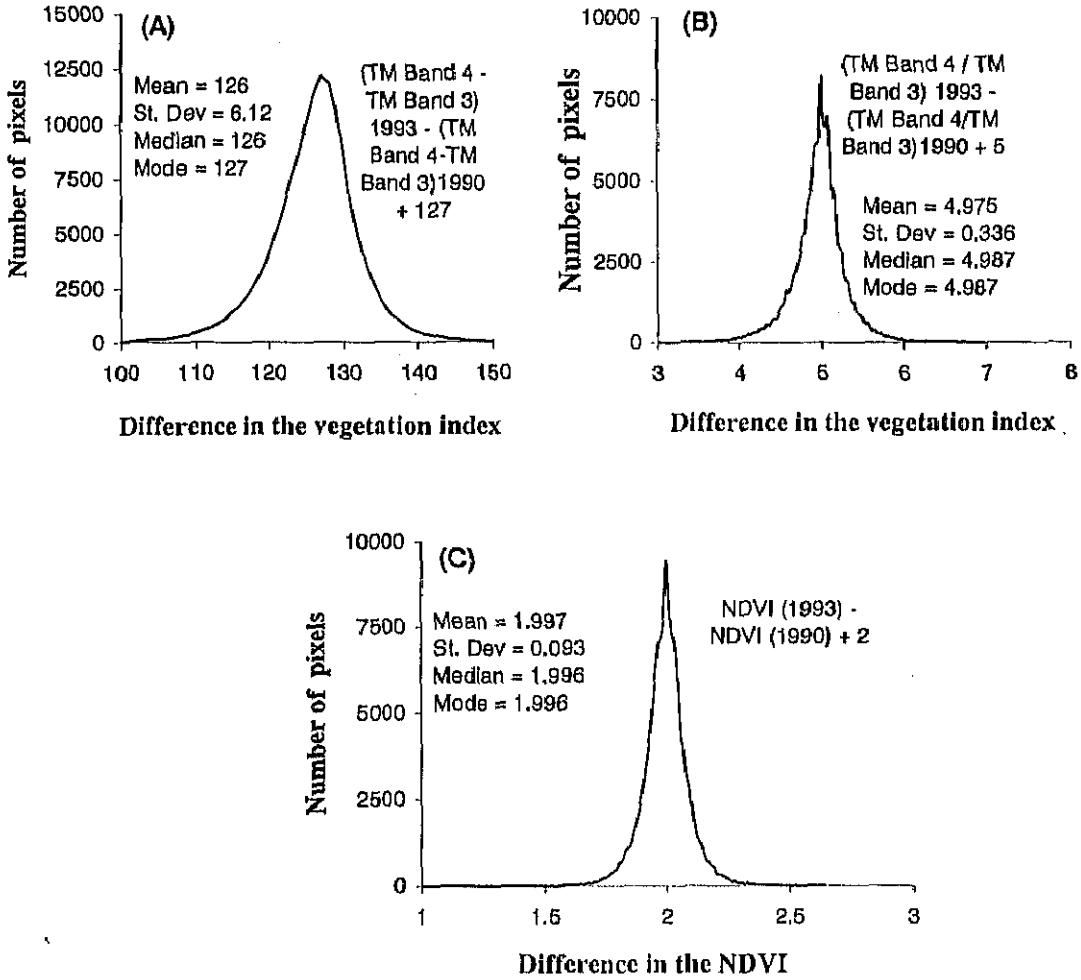

Figure 4-7 (A-C) Histograms of change images for vegetation index image differencing (A) Diffrence vegetation index differencing, (B) Ratio vegetation index differencing, (C) Normalized difference vegetation index (NDVI) differencing.

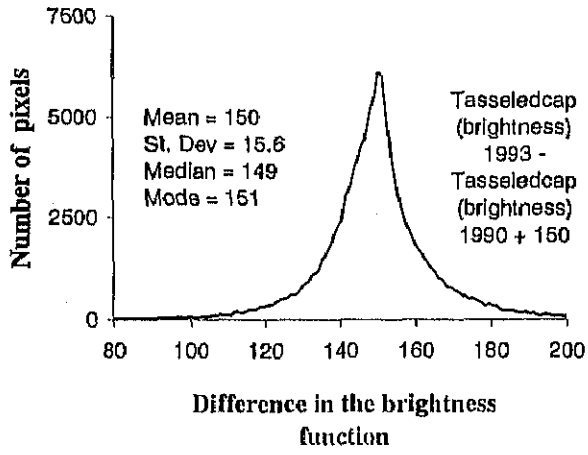

Figure 4-8 Histogram of change image for tasseled cap brightness function.

4-1-3.3 Tasseled cap brightness image differencing

Tasseled cap transformation, also called Kauth and Thomas transformation, was first developed by Kauth and Thomas (1976) using Landsat -MSS data. Crist (1983) and Crist and Cicone (1984) extend the tasseled cap transformation to the Landsat TM data excluding band 6 (Crist and Kauth, 1986). Details on the tasseled cap transformation can be found in Jensen (1996) and Mather (1988). A new coordinate system is defined from this transformation where the characteristics of the remotely sensed data can be more readily viewed. The axes of this new coordinate system are termed "brightness", "greenness" and "wetness". In this study, only the brightness function of tasseled cap transformation was employed, which is a weighted average of the six bands. In three dimensional space, the positions of individual pixels can be computed using the equation 4 as shown below.

$$\text{Brightness} = 0.3037\,(TM1) + 0.2793\,(TM2) + 0.4343\,(TM3) + 0.5585\,(TM4) + 0.5082\,(TM5) + 0.1863\,(TM7) \quad \text{----------(4)}$$

A brightness image was produced from the TM images of 1990 and 1993 using above transformation equations and the 1990 image was subtracted from that of 1993. The ranges of tasseled cap brightness values in 1990 and 1993 vary between 2-231 and 10-321, respectively. The brightness image differences vary between (–91)-127. Considering this range in the difference image a constant value of 150 was added, and a non- negative change image was produced. The values higher than the mean indicate an increase in the brightness in 1993 (see Figure 4-8).

Thresholding and accuracy assessment

The threshold value was determined in the same manner as explained in the preceding sections. The accuracy assessment was carried out using 1,468 no change pixels and 1,075 change pixels, using the right side tail of the histogram.

4-1-3.4 Spectral change vector analysis

When the land undergoes a change due to disturbances, its spectral value changes between dates. If two spectral variables are measured and plotted for the area

both before and after change occurs, it can be expressed by a vector (Jensen 1996). The vector describing the direction and magnitude of change from the first to the second date is a spectral change vector (Malila, 1980; Michalek *et al.*, 1993). The total change magnitude per pixel (CM_{pixel}) is computed by determining the square of the Euclidean distance between the points through *n*-dimensional change space (Malila, 1980; Michalek *et al.*, 1993, Jensen, 1996).

$$CM_{pixel} = \sum_{k=1}^{n} [BV_{i,j,k(date2)} - BV_{i,j,k(date1)}]^2 \quad \text{----------(5)}$$

Where, $BV_{i,j,k(date\,2)}$ and $BV_{i,j,k(date1)}$ are the date 1 and date 2 pixel values in band *k*. A scale factor (e.g., 5) can be applied to each band to magnify small changes in the data if desired. The change direction for each pixel is specified by whether the change is positive or negative in each band. Thus 2^n (where n is the number of bands used) possible types of changes can be determined per pixel (Virag and Colwell, 1987). For example if two bands are used, there are 2^2 or 4 types of changes or sector codes possible, whereas for three bands, there will be 8 possible sector codes (Table 4-4). Let us consider a single registered pixel measured in two bands (band 3 and band 4) on two dates. The change in band 3 was positive with values 45 and 40 for date 2 and date1, respectively. Similarly the change in band 4 was negative with values 40 and 45 for date 2 and date 1, respectively. Then the change magnitude of pixel would be $5^2 + (-5)^2 = 50$. The change sector code or direction for this pixel would be +, -, and will have value 3 (Table 4-4). Two spectral change vector analyses were applied in this study.

i) Three visible bands (band 1: blue, band 2: green, band 3: red) were selected because the preliminary result show that all the three visible bands show abrupt increase in BV in the areas of disturbances (see Table 4-1). A scale factor of five was used in the processing of each TM band. Since three bands were used in this case eight possible types of changes were expected. For the rare instances where pixel values did not differ between two dates, a default direction of "+" was used to ensure that all pixel was assigned a direction. However, only a change of sector 8 was of interest because pixels at this sector code represent the increase in BV in all bands 1, 2 and 3. The landslide affected area result in an increase in a vector magnitude because they often caused erosion or deposition exposing bright sand or coarser sediments. Table 4-5 shows the

Table 4-4 Sector code definitions for change vector analysis processing using three bands, and two bands. "+" indicates the increase in spectral value in 1993 (post disaster scene) and "-" indicates the decrease in spectral value in 1993.

Using three bands 1, 2 and 3				Using two bands 3 and 4		
Sector code	Band 1	Band 2	Band 3	Sector code	Band 3	Band 4
1	-	-	-	1	-	-
2	-	-	+	2	-	+
3	-	+	-	3	+	-
4	-	+	+	4	+	+
5	+	-	-			
6	+	-	+			
7	+	+	-			
8	+	+	+			

Table 4-5 The minimum and maximum magnitudes in eight sector codes for change vector analysis processing with TM bands 1, 2 and 3. Only sector code 8 shows significant higher values. This was the sector of interest.

	Sector codes							
	8	7	6	5	4	3	2	1
Minimum magnitude	377	8	5	19	7	7	4	128
Maximum magnitude	96521	2266	1643	5205	2141	1992	1513	32921

Table 4-6 The minimum and maximum magnitudes in four sector codes for change vector analysis processing with TM bands 3 and 4. Only sector 3 was of interest (see text for the explanation).

	Sector code			
	4	3	2	1
Minimum magnitude	407	160	71	234
Maximum magnitude	104042	40890	18253	60015

minimum and maximum magnitudes for different sector code images. For further analysis only sector code 8 is considered.

ii) Secondly, the spectral change vector of band 3 (blue) and band 4 (near infrared) was applied. It was expected that areas where landslide had occurred would be the one, which showed increase in band 3 and decrease in band 4. In this case also a scale factor of five was used in the processing of both TM bands. Since two bands were used in this case four possible types of changes were expected. For the rare instances where pixel values did not differ between two dates, a default direction of "+" was used to ensure that all pixels were assigned a direction. The sector code 3 (see Table 4-4), which indicates the areas with an increase in band 3, and a decrease in band 4, in 1993, was hypothesized to reveal landslides. The maximum magnitudes for different sector codes indicate that sector code 1 (decrease in band 3 and 4 in 1993), and sector code 4 (increase in band 3 and 4 in 1993) also have high values (see Table 4-6). However, the pixels falling on those sector codes were not considered for further analysis for the obvious reason that such cases can not be expected to occur in the areas of landslides.

Thresholding and accuracy assessment

In order to locate the areas undergone changes due to disturbance the threshold values were adopted over the scaled images and the accuracy assessment was carried out. The histograms of the change vector analysis do not have normal distribution but have the only one right side tail. The method for determining the optimal threshold is the modification of the method for a normally distributed histogram. Michalek *et al.* (1993) determined the threshold by examining deep-water areas. The threshold value preliminary determined in this study by examining the deepest part of the water areas (reservoir), did not perform well because it contained a large number of insignificant change pixels. Hence, the threshold level was selectively modified to the upper magnitudes, until it gave the highest accuracy. Accuracy assessments were carried out using 1,468 no change pixel and 1,075 change pixels in the first case (which use bands 1, 2 and 3) to determine the landslide affected areas. In the second case which uses bands 3 and 4, accuracy assessment was carried out using 1,468 no change pixels and 388 landslide pixels, with the expectation of obtaining landslides in the vegetative areas.

4-1-3.5 Principal component analysis

Principal component analysis (PCA), or the Karhunen-Loeve (K-L) transformation (Duvernoy and Leger, 1980), is a multivariate statistical technique. The data axes are rotated into principal axes, or components, that maximize data variance. In this manner correlated data sets can be represented by a small number of axes, while maintaining most of the variation of the original data. A detailed explanation of PCA for the use of remotely sensed data can be found in Mather (1988) and Jensen (1996).

PCA in this study was based on bands 1, 2, and 3 merged data set from the images of 1990 (pre-disaster) and 1993 (post disaster). The basic premise for PCA with merged data in change detection is that one or more of the new PCA bands contain information that can be directly related to change (Byrne *et al.*, 1980; Jensen, 1996; Dobson *et al.*, 1995). Muchoney and Haack (1994), for example, demonstrated that multitemporal SPOT spectral information related to hardwood defoliation by gypsy moths was confined to a single PCA band (3).

The 6 x 6 covariance matrix of the 6 dimensional merged remote sensing data set to be transformed, was computed. The eigenvalues and eigenvectors of the covariance matrix were computed (Table 4-7). The first, second, and third principal components account for 96.16, 2.81 and 0.87 percent of the variance, respectively. Principal component images were computed from the eigenvectors much in the same way as the tasseled cap transformation was derived from its components. Analysis of the eigenvector of the transformed data, and visual inspection of six images, indicated a third component image best representing the areas affected by landslides. An arbitrary value of 60 was added to produce a non-negative image, and further analysis was done only with the image produced from the third principal component.

Thresholding and accuracy assessment

The threshold value that separates the pixels of change from those of no change was determined by carrying out two steps as explained in the preceding sections (section 4-1-3.1). Accuracy assessment was carried out using 1,468 no change pixels and 1,075 change pixels. Since the areas affected by landslides corresponded with the values less than the mean only the pixels falling on the left side tail of the histogram (Figure 4-9) were considered for thresholding and accuracy assessment.

Table 4-7 Eigenvectors and eigenvalues computed from the covariance matrix for the principal component analysis.

Year/Band		Component P					
		1	2	3	4	5	6
1993	1	0.584	-0.374	-0.377	-0.565	-0.198	-0.135
	2	0.251	0.135	-0.281	0.009	0.452	0.797
	3	0.329	0.592	-0.509	0.400	-0.093	-0.336
1990	1	0.568	-0.389	0.372	0.613	-0.088	0.062
	2	0.245	0.102	0.284	-0.176	0.790	-0.440
	3	0.324	0.574	0.548	-0.336	-0.340	0.191
Eigenvalues		1913.419	55.886	17.299	1.705	1.065	0.433
% Variance		96.16	2.81	0.87	0.09	0.05	0.02
% Cumulative Variance		96.16	98.97	99.84	99.92	99.98	100.00

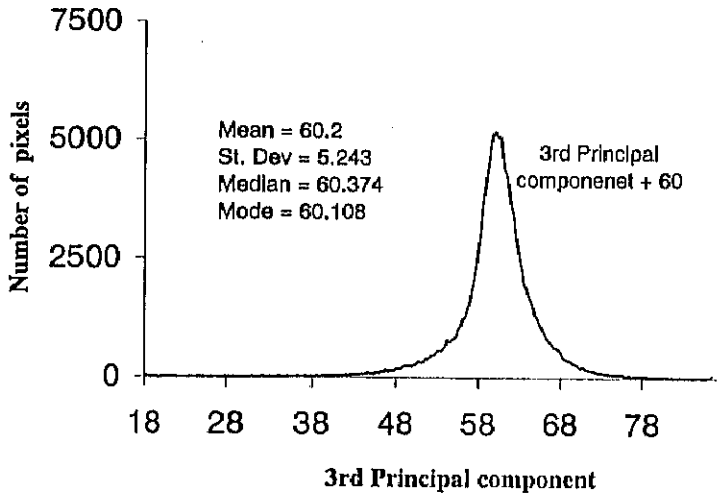

Figure 4-9 Histogram of the 3rd principal component image.

4-2 RESULTS

4-2-1 Spectral Image Differencing

Threshold value of the standard deviation x N to the mean, with the starting value of N = 0.25 and the increment of 0.25 until N = 3.0, and the corresponding change pixels are depicted in Table 4-8. The shaded portion is the range of the threshold in which accuracy assessment was performed to determine the optimal threshold as explained in the section 4-1-3.1. Figure 4-10 (A-D) show the change images depicting change pixels by different bands at different threshold values.

Four change images had the optimal threshold at N = 1, and they have different accuracies in detecting areas affected by landsliding. Both overall accuracy and Khat were found highest at N = 1 (Table 4-8). Among the four spectral images differencing employed, band 2 has the highest accuracy with 87.5 percent and 74.2 percent overall and Khat accuracies respectively, in differentiating between the areas affected from not affected. In terms of the accuracies, band 2 image differencing was followed by band 1 and band 3 images differencing. Band 7 gave the lowest accuracy.

4-2-2 Vegetation Index Image Differencing

In this study vegetation indices were expected to reveal disturbances in the vegetated areas by landsliding. The accuracy assessment was carried out using 1,468 no change pixels and 388 landslide pixels. Table 4-9 shows the threshold values and the accuracies at different thresholds. Figure 4-11(A-C) shows the change images, depicting the change pixels by different vegetation indices at a different threshold.

The three vegetation index change images have different threshold and different accuracies (Table 4-9). Both overall accuracy and Khat were comparatively low when compared to the spectral image differencing. NDVI has the highest accuracy for vegetation responses to landsliding with 84.8 percent and 52.7 percent overall and Khat accuracies, respectively, at threshold N =1.25.

4-2-3 Tasseled Cap Brightness Image Differencing

Figure 4-12 shows the change images depicting the change pixels by different tasseled cap brightness functions at different threshold. Threshold values and the corresponding number of change pixels are shown on Table 4-10. The shaded portion is

Table 4-8 Threshold values and change pixel corresponding to value of the standard deviation x N to the mean (N = 0.25-3.0) for bands 1, 2, 3, and 7 change images. The shaded portion is the range of threshold depicting pixels affected by landsliding. The accuracy assessment based on the overall accuracy and the Khat was performed to decide the threshold from this range.

Threshold parameter	Band 1				Band 2				Band 3				Band 7			
	TV (>)	Acc. %		Pixel number	TV (>)	Acc. %		Pixel number	TV (>)	Acc. %		Pixels number	TV (>)	Acc. %		Pixel number
		OA	Kh			OA	Kh			OA	Kh			OA	Kh	
Mean + 0.25 st. dev	129			39866	127			54921	128			41939	130			47730
Mean + 0.5 st. dev	130			27635	128			33571	129			31357	132			28218
Mean + 0.75 st.dev	131			19438	129			21182	131			19543	134			20794
Mean + 1 st. dev	132	87.0	72.6	13951	130	87.5	74.2	14285	132	86.0	70.5	15877	136	82.9	63.5	15467
Mean + 1.25 st. dev	133	86.1	70.5	10234	131	86.6	71.4	9867	134	84.1	66.0	10652	138	80.8	58.6	11671
Mean + 1.5 st. dev	134	85.3	68.7	7762	131	86.6	71.4	9867	135	82.7	62.6	8824	140	79.0	54.3	8816
Mean + 1.75 st. dev	135	84.2	66.0	6057	132	83.9	65.4	6969	137	81.4	59.8	7321	142	76.8	49.0	6667
Mean + 2 st. dev	136	83.0	63.2	4799	133	81.6	59.9	4955	138	78.5	52.8	4953	144	74.4	43.0	5016
Mean + 2.25st. dev	138	80.0	56.3	3126	134	79.2	54.5	3598	139	77.4	50.1	4126	146	71.9	36.9	3782
Mean + 2.5 st. dev	139			2637	135			2697	141			3456	148			2814
Mean + 2.75 st. dev	140			2188	136			2006	142			2371	150			2139
Mean + 3 st. dev	141			1863	137			1530	144			1699	152			1566

TV: Threshold value, Acc.: Accuracies, OA: Overall accuracy, Kh: Khat accuracy

Table 4-9 Threshold values, accuracies and pixel number corresponding to the different values of the standard deviation x N to the mean for the three vegetation index change images.

Threshold parameter	Difference Vegetation index (Band 4 - Band 3)				Ratio vegetation index (Band 4 / Band 3)				NDVI (Band 4 - Band 3 / Band 4 + Band 3)			
	TV (<)	Acc. %		Pixel number	TV (<)	Acc. %		Pixel number	TV (<)	Acc. %		Pixel number
		OA	Kh			OA	Kh			OA	Kh	
Mean-0.25 st. dev	125			47618	4.891			47425	1.973			51193
Mean-0.5 st. dev	123			31681	4.807			33773	1.950			37813
Mean-0.75 st. dev	122			25611	4.723			24263	1.927			27500
Mean-1 st. dev	120	83.7	50.1	16574	4.639	83.0	48.3	17436	1.904	84.8	52.7	19931
Mean-1.25 st. dev	119	83.6	47.7	13395	4.555	83.8	48.3	12566	1.880	86.2	53.3	12218
Mean-1.5 st. dev	117	83.9	44.6	8705	4.471	84.5	47.1	9158	1.855	85.7	48.9	8823
Mean-1.75 st. dev	116	83.7	41.2	7040	4.387	84.5	44.8	6832	1.834	85.2	44.3	6479
Mean-2 st. dev	114	83.8	38.1	4525	4.303	84.1	41.6	5100	1.811	84.3	38.7	4669
Mean-2.25 st. dev	113	83.3	34.1	3653	4.219	83.8	38.6	3501	1.787	84.1	35.5	3835
Mean-2.5 st. dev	111			2390	4.135			2640	1.764			2050
Mean-2.75 st. dev	109			1584	4.051			1837	1.741			1469
Mean-3 st. dev	108			1270	3.967			1509	1.718			1035

TV: Threshold value, Acc.: Accuracies, OA: Overall accuracy, Kh: Khat accuracy

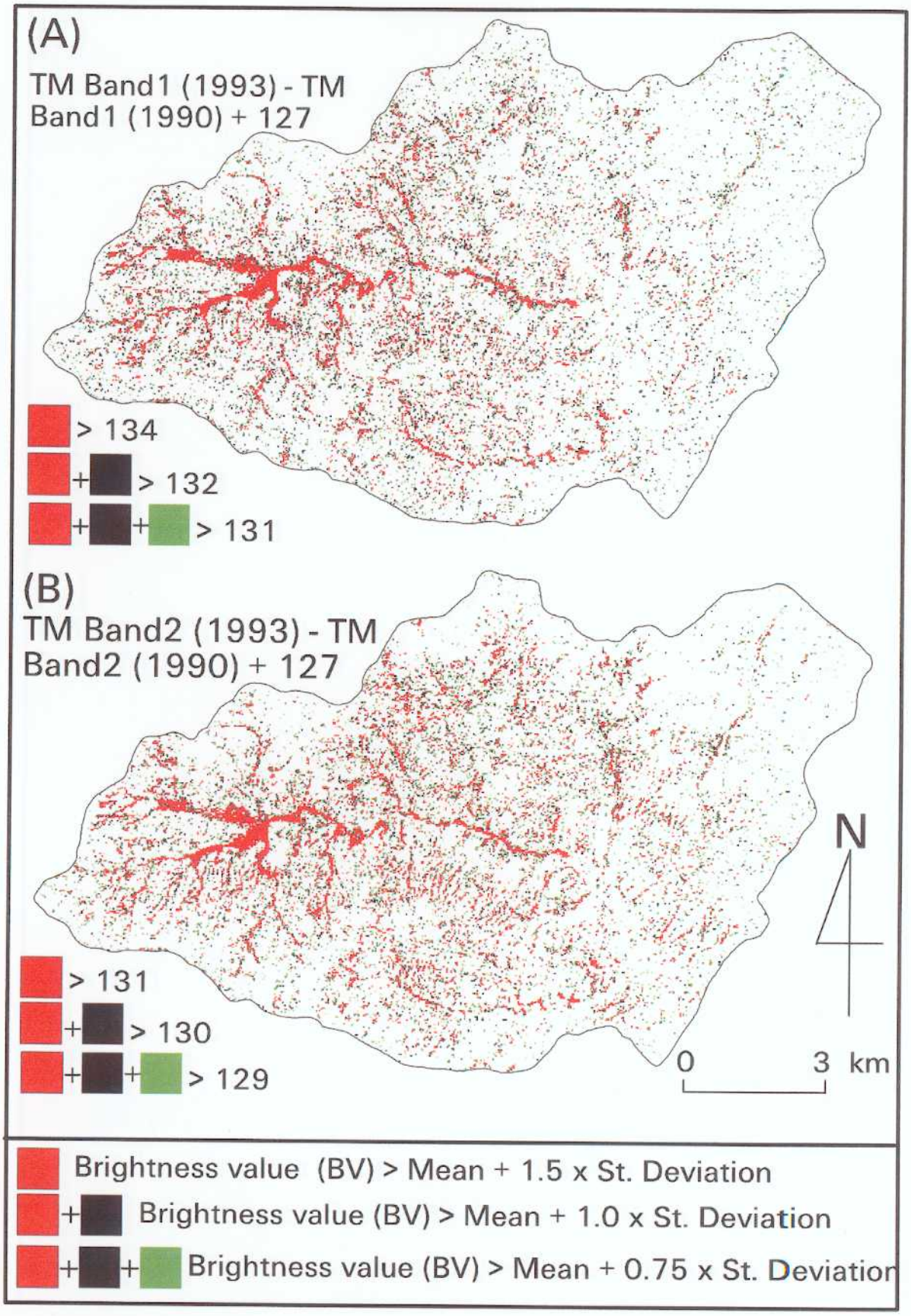

Figure 4-10 (A-D) The results of the spectral image differencing showing change pixels at different threshold values using the standard deviation (St. Deviation) and the mean. Highest accuracies were obtained at one standard deviation to the mean (N = 1).

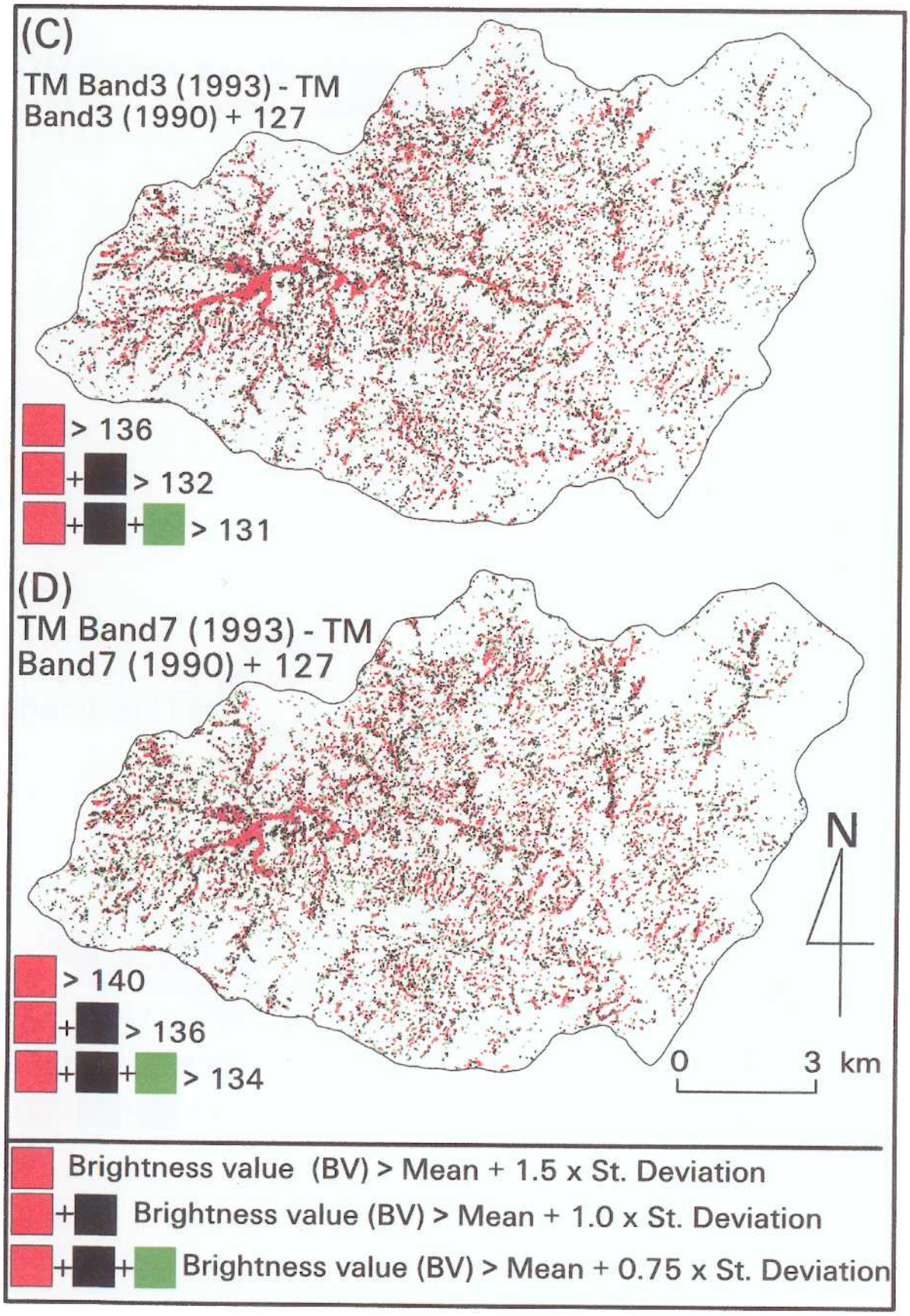

Figure 4-10 (continued).

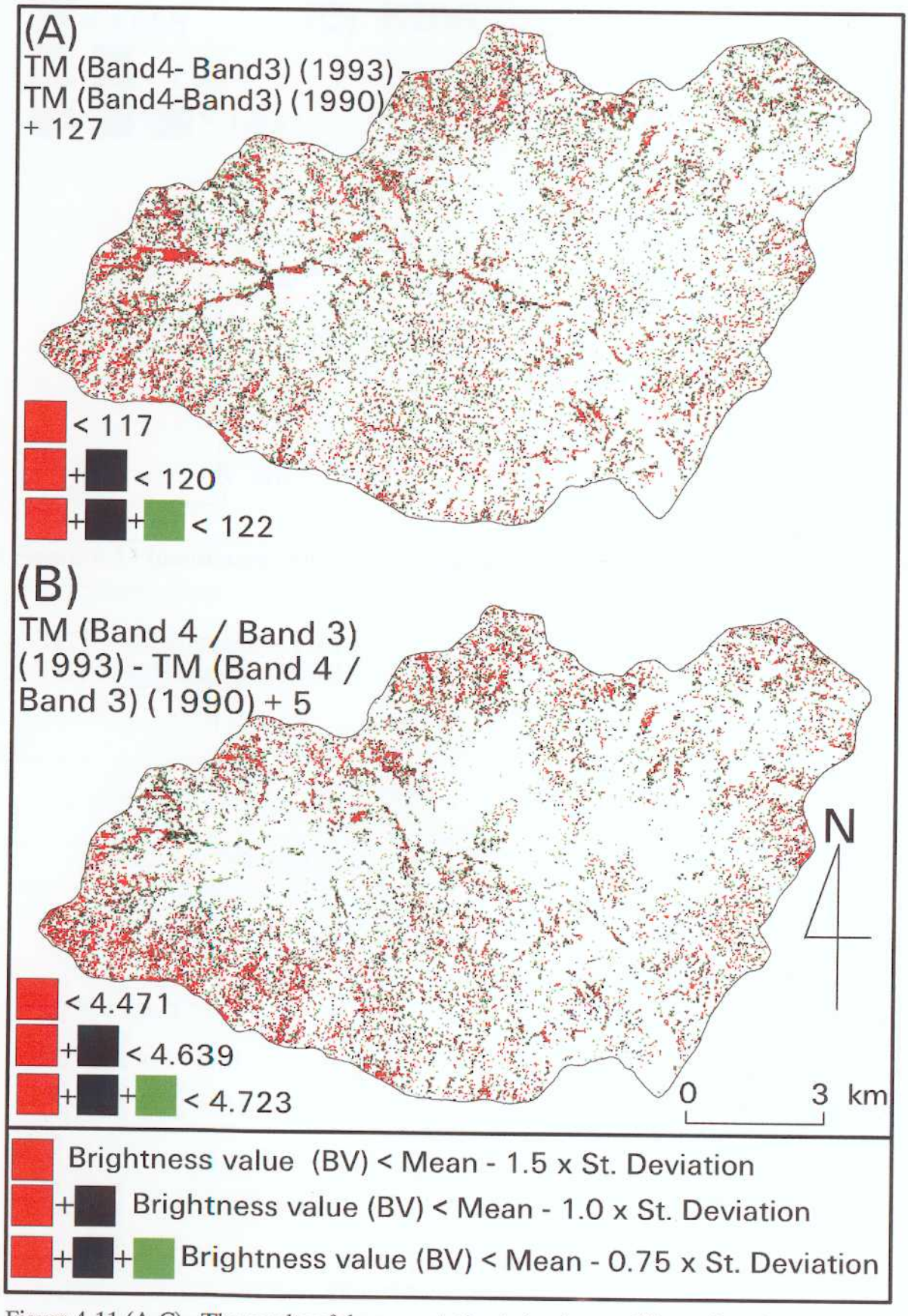

Figure 4-11 (A-C) The results of three vegetation index image differencing showing change pixels at different threshold values using the standard deviation (St. Deviation) and the mean.

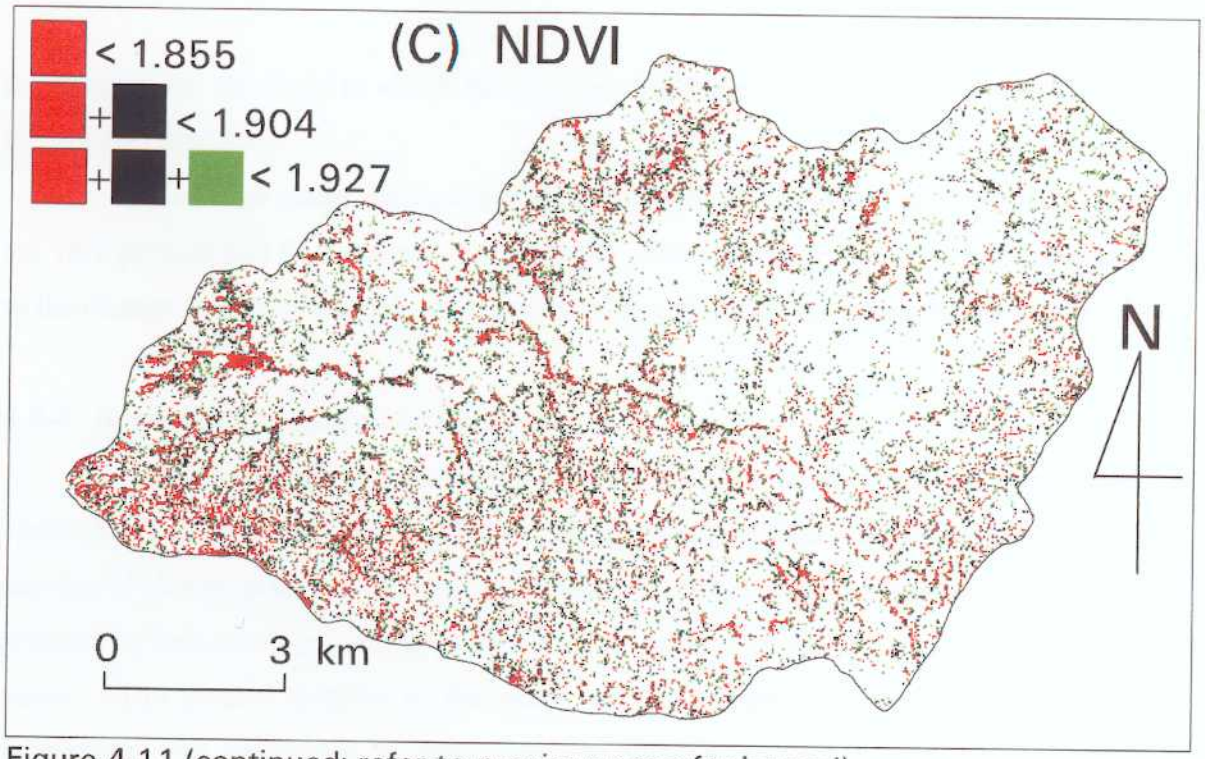

Figure 4-11 (continued; refer to previous page for legend).

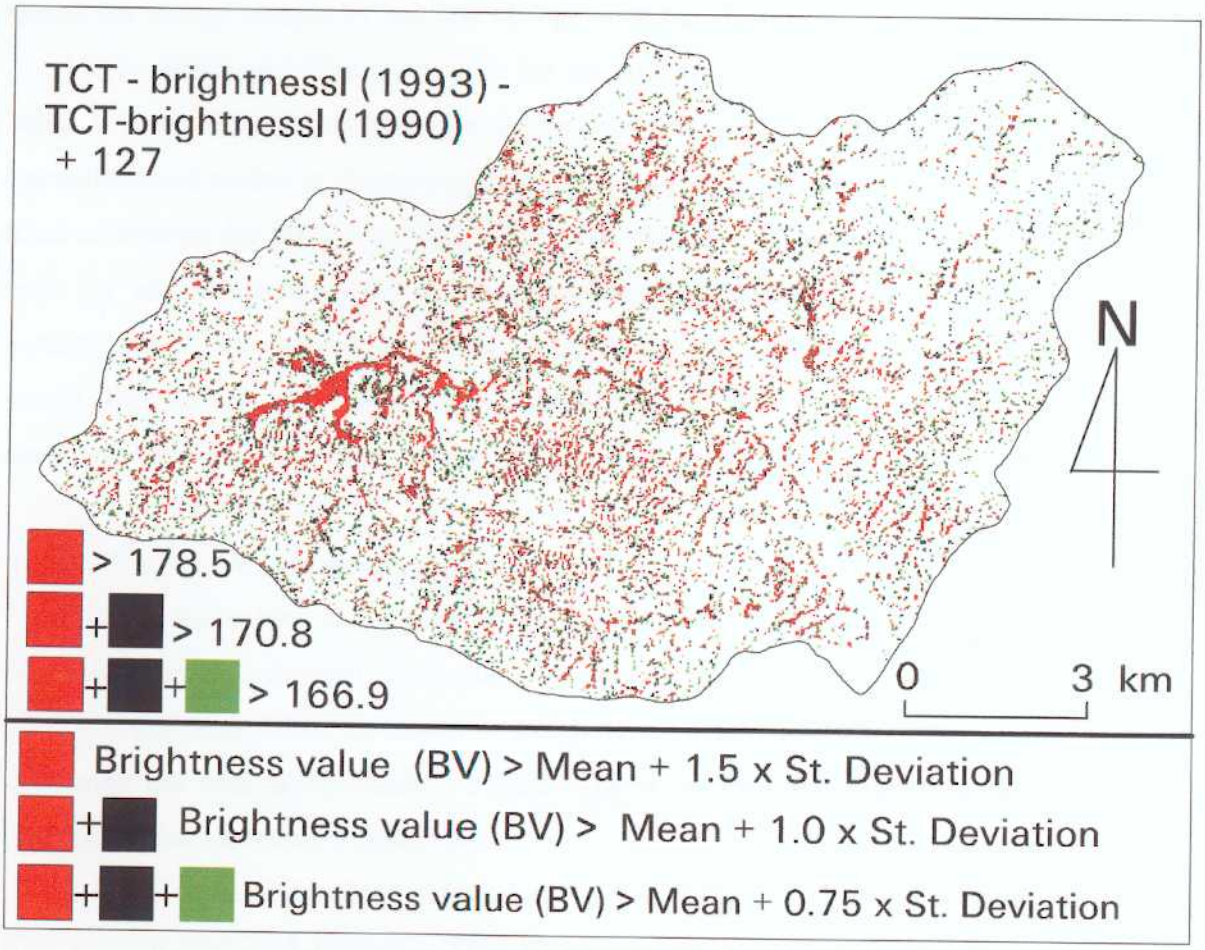

Figure 4-12 The result of the tasseled cap brightness image differencing showing change pixels at different threshold values using the standard deviation (St. Deviation) and the mean.

the range of the threshold in which the accuracy assessment was performed to determine the optimal threshold.

The change image has optimal threshold at N = 1. Overall and Khat accuracies are 78.7 percent and 54.1 percent, respectively. The accuracies are very low compared to the change images produced from spectral image differencing (using bands 1, 2, 3).

4-2-4 Spectral Change Vector Analysis

Two spectral change vector analyses that used three bands (1, 2 and 3), and two bands 3 and 4 were applied in this study. Threshold values and the corresponding number of change pixels are shown on Table 4-11. The threshold values in this case are selected by subjective judgement until a realistic amount of change was obtained in the scene. The shaded portion is the range of the threshold in which the accuracy assessment was performed to determine the optimal threshold. Figure 4-13 (A-B) shows the change images by spectral change vector analysis.

The overall and Khat accuracies for the spectral change vector analysis that used bands 1, 2, and 3 (sector code 8) which was expected to reveal the overall affected areas (landslides and sediment deposition) are 88.3 percent and 75.4 percent. The overall and Khat accuracies for the spectral change vector analysis that used bands 3 and 4 (sector code 3), which was expected to reveal disturbances in the vegetated areas are 81.4 percent and 35.7 percent respectively. The former gave high accuracies than spectral image differencing and tasseled cap transformation. The later however, gave lower accuracies when compared to vegetation index image differencing.

4-2-5 Principal Component Analysis

Threshold values and the corresponding accuracies and the number of change pixels for the 3rd principal component image are shown on Table 4-11. The shaded portion is the range of the threshold in which the accuracy assessment was performed to determine the optimal threshold. Figure 4-14 is the 3rd principal component image depicting areas affected by landslides.

The optimal threshold is found at N = 1 with the overall and Khat accuracies of 87.4 percent and 73.4 percent. This accuracies are very close to the accuracies of spectral change vector analysis (bands 1, 2 and 3) and band 2 image differencing.

Table 4-10 Threshold values, accuracies and pixel number corresponding to the different values of the standard deviation x N to the mean for tasseled cap brightness function change image.

Threshold parameter	Tasseled Cap (Brightness)			
	TV (>)	Accuracies		Pixel number
		OA	Khat	
Mean+0.25st. dev	154.2			41180
Mean+0.5 st. dev	158.1			29541
Mean+0.75 st. dev	162.0			21763
Mean+1 st. dev	165.9	78.7	54.1	15013
Mean+1.25 st. dev	169.8	76.9	49.7	11392
Mean+1.5 st. dev	173.7	75.6	46.3	8064
Mean+1.75 st. dev	177.6	73.7	41.5	6115
Mean+2 st. dev	181.5	72.1	37.5	3639
Mean+2.25 st. dev	185.4	70.8	34.2	3417
Mean+2.5 st. dev	189.3			2626
Mean+2.75 st. dev	193.2			2143
Mean+3 st. dev	197.1			1463

TV: Threshold value, Acc.: Accuracies, OA: Overall accuracy, Kh: Khat accuracy

Table 4-11 Threshold values, accuracies and pixel number corresponding to different subjectively selected threshold values for two spectral change vector analysis. The results of principal component analysis is also listed.

Three bands 1, 2 and 3				Two bands 3 and 4				Principal Component Analaysis (PC 3)				
TV (>)	Accuracies		Pixel number	TV (>)	Accuracies		Pixel number	Threshold parameter	TV (>)	Accuracies		Pixel number
	OA	Khat			OA	Khat				OA	Khat	
							40771	Mean-0.25st. dev	58.89			43192
							31427	Mean-0.5 st. dev	57.58			27407
1513	88.3	75.4	16270				24156	Mean-0.75 st. dev	56.27			19190
1891	88.0	74.7	14295				18526	Mean-1 st. dev	54.97	87.4	73.4	14137
2270	87.6	73.8	12424	640	81.4	35.7	14226	Mean-1.25 st. dev	53.65	86.1	70.5	10566
2648	87.2	72.9	11243	800	81.7	36.3	8540	Mean-1.5 st. dev	52.34	84.5	66.7	7977
3027	86.8	72.0	10174	961	82.7	38.2	6669	Mean-1.75 st. dev	51.02	82.4	61.9	6117
3504	86.6	71.5	9193	1121	82.7	37.6	5258	Mean-2 st. dev	49.71	80.5	57.4	4977
3784	86.1	70.3	8387	1281	82.7	36.5	4162	Mean-2.25 st. dev	48.40	78.0	51.6	3802
4162	85.2	68.3	7578				2632	Mean-2.5 st. dev	47.09			2973
							2087	Mean-2.75 st. dev	45.78			2316
							1663	Mean-3 st. dev	44.47			1858

TV: Threshold value, Acc.: Accuracies, OA: Overall accuracy, Kh: Khat accuracy

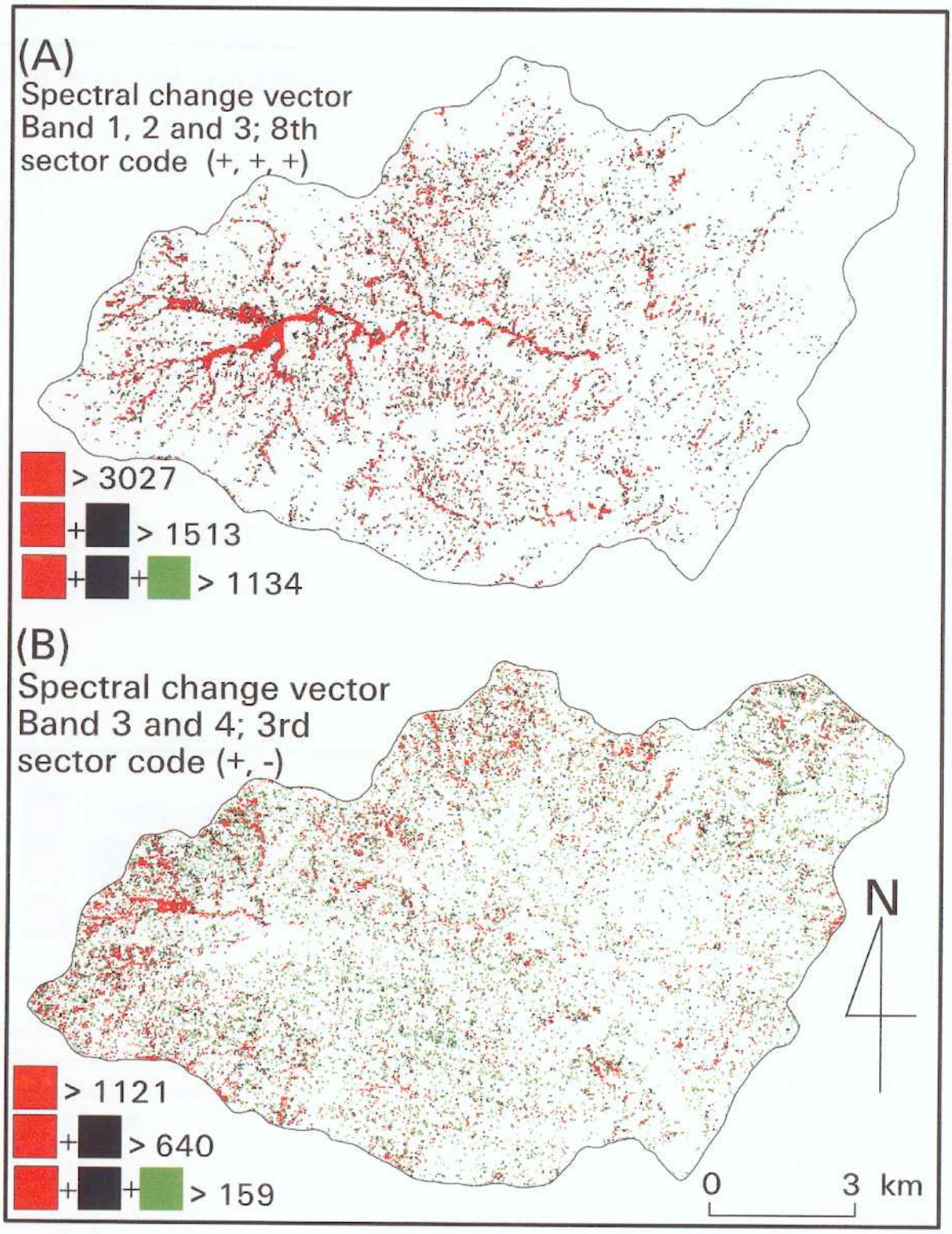

Figure 4-13 (A-B) The results of the spectral change vector analysis showing change pixels at different threshold values. The values were subjectively selected by trial and error in order to find the optimal threshold value.

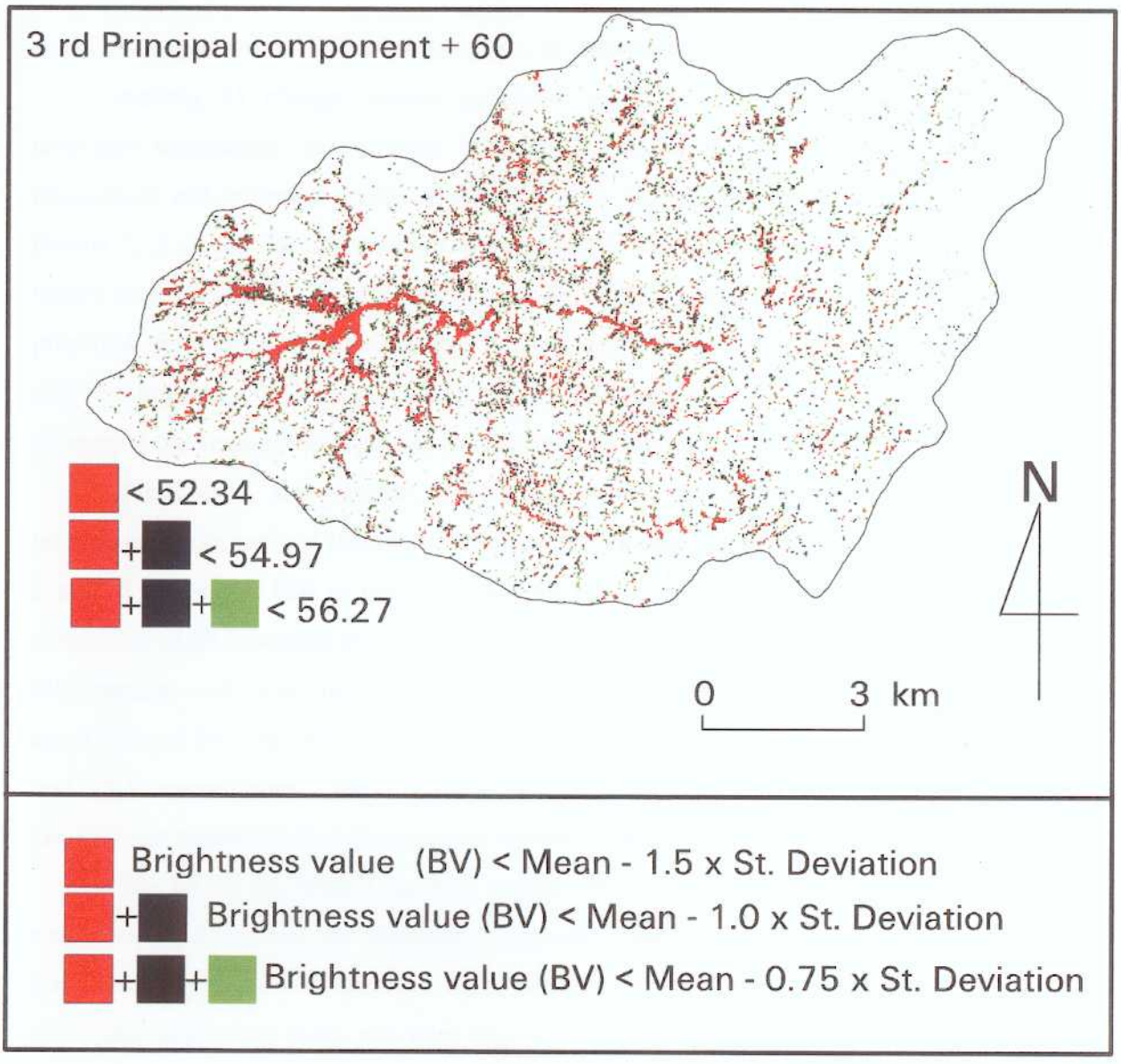

Figure 4-14 The result of the principal component image analysis showing change pixels at different threshold values. The third principal component image represented for the areas affected by landslides. The change pixels shown are detected from the third principal component image.

4-2-6 Comparison of Different Methods in Differentiating Change vs. No Change

Among 11 change images generated using five different kinds of change detection techniques, seven were expected to reveal the landslide affected areas (landslides and sediment deposited areas). They include four spectral change images (bands 1, 2 ,3 and 7), one tasseled cap brightness change image, one spectral change vector image (bands 1, 2 and 3: sector code 8), and one principal component image (3^{rd} principal component). Four change images, generated form three vegetation index differencing and one spectral change vector analysis (bands 3 and 4), were used to determine the vegetation responses to disturbances caused by landsliding.

Table 4-12 summarizes the accuracies for the different change detection techniques at the optimal threshold. The spectral change vector analysis (using bands 1, 2 and 3) performed best to detect the overall affected areas with the overall and Khat accuracies of 88.3 percent and 75.4 percent respectively. Band 2 (green) spectral image differencing and principal component analysis were the next best with overall accuracies of 87.5 percent and 87.4 percent, respectively, and Khat accuracies of 73.6 and 73.4, respectively. Band 7 (mid infrared) spectral image differencing and the tasseled cap transformation (brightness) showed least accuracies.

The NDVI performed the best among the four algorithms that were specially employed to determine the vegetation responses due to landsliding. The overall and Khat accuracies are 86.2 percent and 53.3 percent respectively. The accuracies of difference vegetation index and ratio vegetation index are close to NDVI. However, as expected before the analysis, the spectral change vector analysis using bands 3 and 4 did not give better accuracies.

4-2-7 Detecting Different Kinds of Affected Areas Associated with Landsliding

Two change images produced using the change vector analysis and the NDVI, which gave the highest accuracy in determining landslide affected areas or vegetation responses to landsliding, respectively, are depicted in Figure 4-15 (A-B). These images give the information regarding the affected areas associated with landsliding. In other word the techniques determine whether or not the area has been affected by landsliding. The pixels need to be classified when we need the information regarding the type of change. For example, landslide affected areas consist of areas with landslides, debris

Table 4-12 Comparison of the accuracies of different change detection methods at the optimal threshold. Spectral change vector analysis using bands 1, 2, and 3 performed best for detecting landslide affected areas (landslides/sediment deposition). NDVI performed best to detect the vegetation responses to landsliding.

Change detection method (employed for the identification of Overall affected areas)			Producer's Accuracy		User's accuracy		Change detection method (employed for the identification of vegetation responses caused by landslides)			Producer's accuracy		User's accuracy	
	OA	Kh	No Change	Change	No Change	Change		OA	Kh	No Change	Change	No Change	Change
SID Band 1	87.0	72.6	96.1	74.5	83.7	93.4	VIID Difference	83.7	50.1	90.2	59.3	89.3	61.5
SID Band 2	87.5	73.6	96.2	75.5	84.3	93.5	VIID Ratio	83.8	48.3	91.9	53.6	88.1	63.8
SID Band 3	86.0	70.5	95.4	73.2	82.9	92.0	VIID NDVI	86.2	53.3	95.0	52.8	88.4	73.5
SID Band 7	82.9	63.5	96.0	65.0	78.9	92.2	SCVA Bands 3 and 4 (sector code 3)	82.7	38.2	94.5	37.9	85.2	64.5
TCTID Brightness	78.7	54.1	95.4	56.0	74.7	89.9							
SCVA Bands 1, 2, and 3 (sector code 8)	88.3	75.4	95.4	78.5	85.9	92.5							
PCA (PC 3)	87.4	73.4	96.9	74.4	83.8	94.7							

SID: Spectral image differencing, VIID: Vegetation index image differencing, TCTID: tasseled cap transformation image differencing, SCVA: Spectral change vector analysis, PCA: Principal component analysis, OA: Overall accuracy, Kh: Khat accuracy.

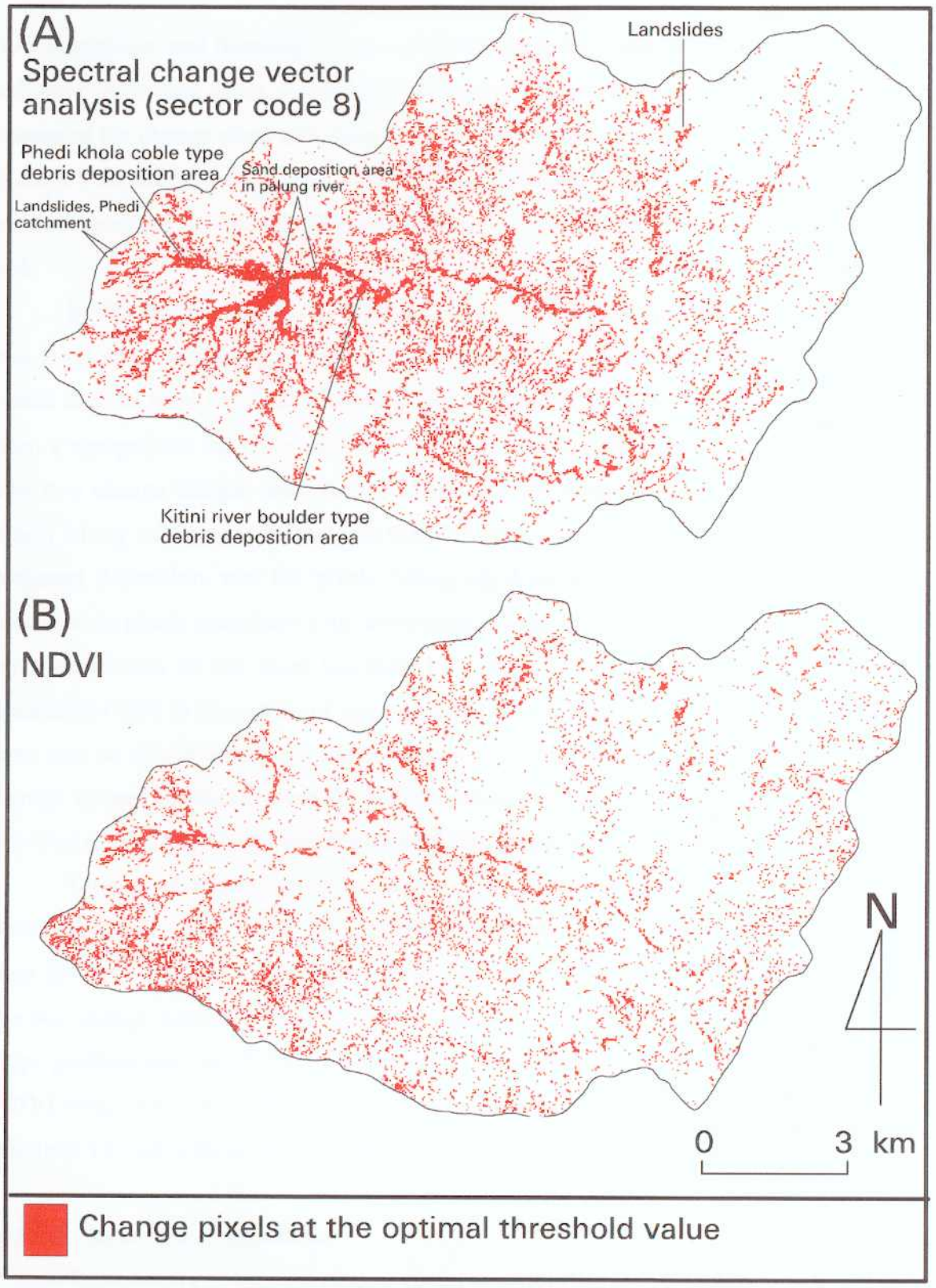

Figure 4-15 (A-B) Change pixels at the optimal threshold value detected by two best change detection methods. Spectral change vector (sector code 8) depicts the landslide affected areas and NDVI depicts the vegetation responses to landsliding.

flow deposition, and flooding. If we can differentiate the pixels of landslides to that of sediment deposition areas, it would be of great value. In Figure 4-15(A) some of the classes of the change areas have been mentioned from the fieldwork data (see Figure 2-3 also). To classify all the change pixels into different classes, some classification method needs to be applied. The classification of these pixels however, is a difficult task.

In this study a broad classification system was applied to classify change pixels into areas with landsliding or sediment deposition. For this purpose a digital elevation model derived from the Triangulation Irregular Network (TIN) using digitized contours from a topographic map (see section 5-1-1) was used to produce a slope gradient map. The two change images were then masked with the slope gradient map and change pixels falling on a slope gradient less than 15° were classified as pixels associated with sediment deposition, and the pixels falling on slope gradient greater than 15° were classified as pixels associated with landsliding. It is generally accepted that a deposition processes occurs on the slope less than 15°, and it is also common to find landslide phenomena only in the region of slope gradient greater than 15°, which was true in this case also as shown by the landslides measured in the field (see Figure 2-6). The two change images produced using the spectral change vector analysis and the NDVI are depicted in Figure 4-16 (A) and Figure 4-16 (B), respectively.

Table 4-13 shows the similar numbers of pixels associated with landsliding in both the change maps. About 40 percent of the pixels located at slope gradient greater than 15° were common in both the change maps indicating a large number of pixels in the two change maps depicting different kinds of change. Since, most of the areas with slope gradient less than 15° in the study areas can be categorized as non vegetated areas, NDVI image was not expected to depict all the changes in the areas with slope gradient less than 15°; consequently these pixels were excluded.

4-2-7.1 Detection of landslides

The capacity of spectral change vector analysis (bands 1, 2 and 3), and NDVI in detecting landslides was examined, because they gave the highest accuracy for detecting landslide affected areas and vegetation responses to landsliding, respectively. Figure 4-17 (A-B) shows the landslide distribution map masked with both the change image of

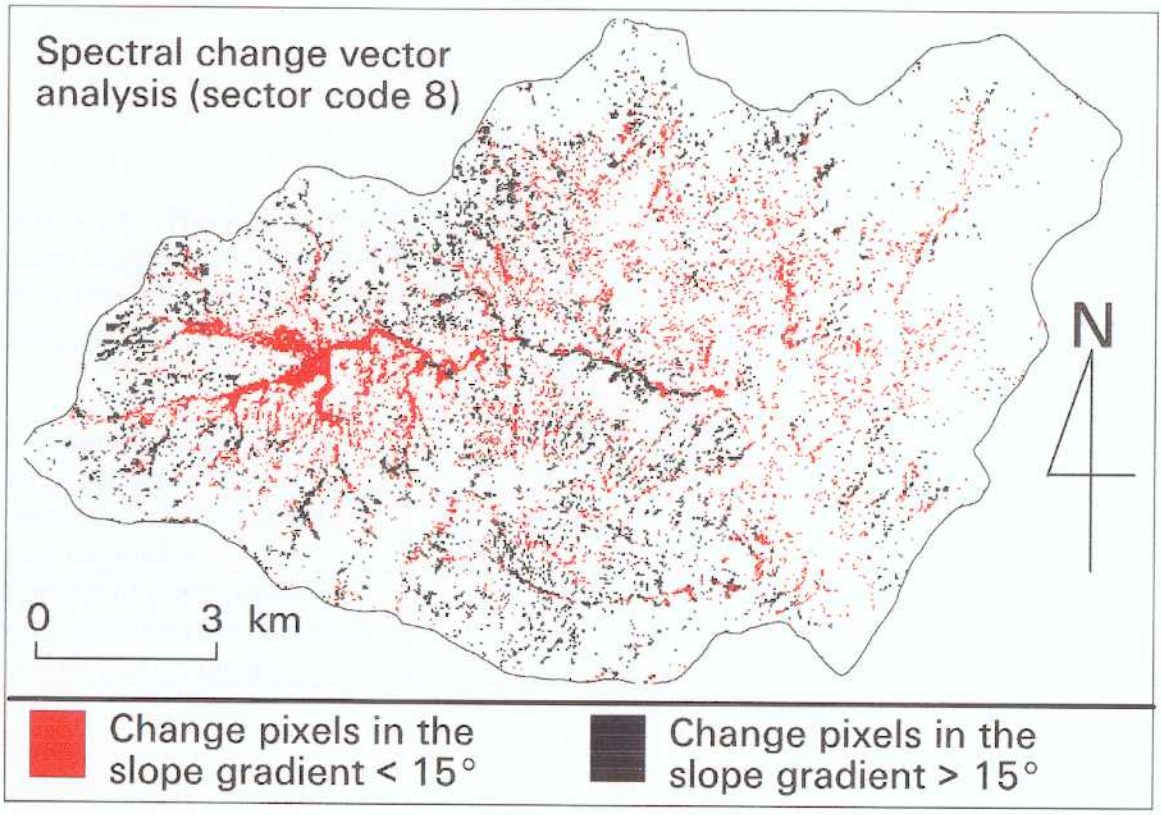

Figure 4-16 (A) Change areas depicted by spectral change vector analysis (sector code 8) by slope gradient.

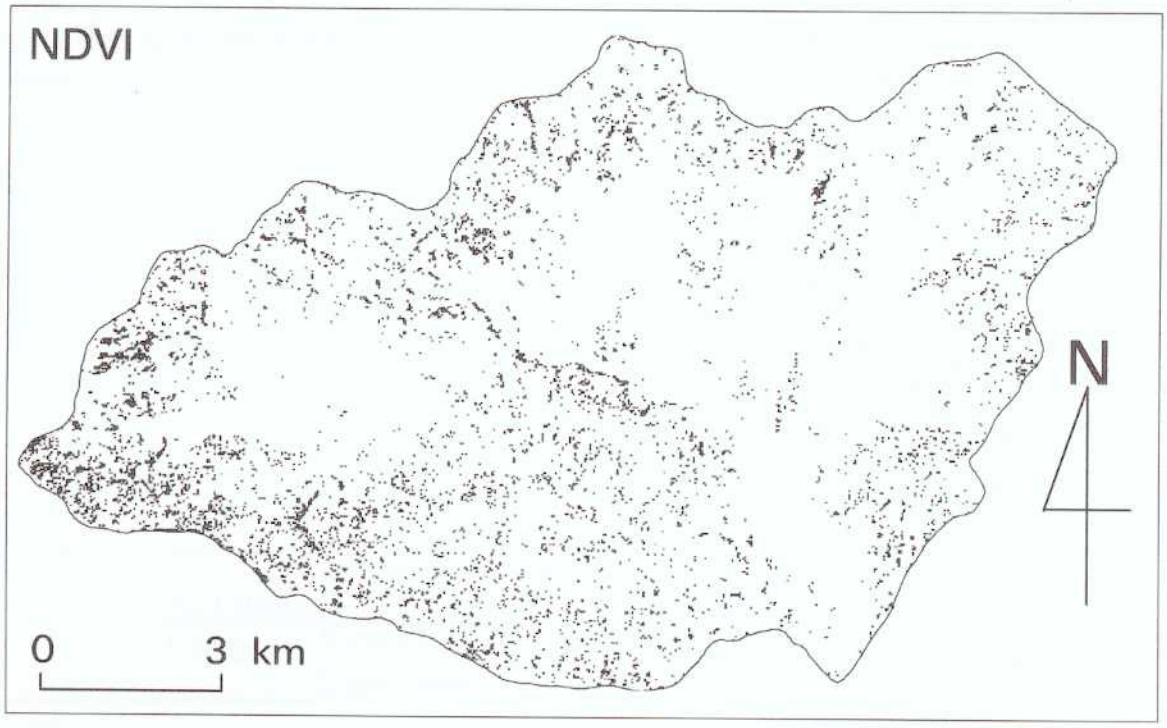

Figure 4-16 (B) Change areas depicted by NDVI. Black spots are the change pixels in the slope gradient greater than 15° (see text for the illustration).

Table 4-13 Number of pixels depicted as sediment deposition or landslides by two change images. NDVI was not expected to reveal changes in non vegetated areas. The pixels that fall in the category of slope gradient < 15° are basically non vegetated area hence, such pixels were discarded.

	Spectral change vector analysis (sector code 8)	NDVI
Number of pixels associated with sediment deposition	8777	-
Number of pixels associated with landslides	7493	7236
Number of pixels associated with landslides and common to both change images	2277	2277

Table 4-14 Modified error matrix generated for the spectral change vector analysis (bands 1, 2 and 3; sector code 8), which produced highest accuracy among the change detection methods employed. The matrix was generated to see the capability of the algorithm to detect different types of changes as landslides and sediment deposition areas.

			Reference data			
			No Change	Change		Total
				Deposition	Landslides	
Classified data	No Change		1400	83	145	1628
	Change	Deposition	37	556	23	616
		Landslides	31	48	220	299
		Total	1468	687	388	2543

	Overall accuracy		0.856		
	Khat		0.745		
	Producer's accuracy			User's accuracy	
No Change		0.954	No Change		0.860
Change	Deposition	0.809	Change	Deposition	0.903
	Landslides	0.567		Landslides	0.736

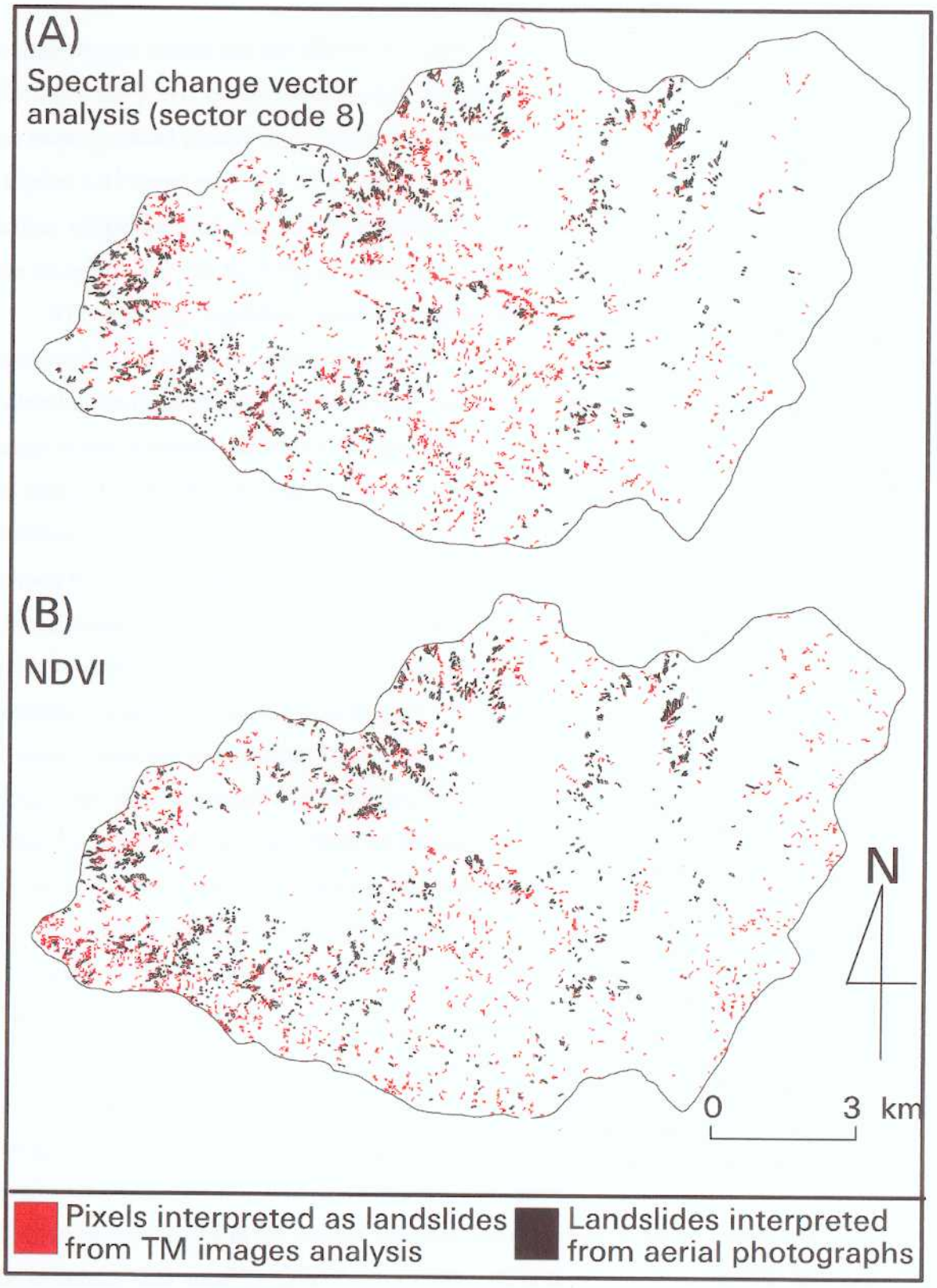

Figure 4-17 (A-B) Comparison of landslides interpreted from the multitemporal TM data using spectral change vector and NDVI, and produced from the interpretation of large scale aerial photographs.

spectral change vector and the NDVI for pixels falling on a slope gradient greater than 15°. Since the pixels on the change image of spectral change vector and NDVI, falling on a slope gradient greater than 15°, also contained pixels from the rivers, those pixels in Figure 4-17 were excluded by masking that with the river layer produced in GIS. In addition single isolated change pixels were excluded because a large number of them were recognized as due to errors of rectification and registration.

The complete landslide distribution map was produced from large-scale aerial photographs (1:20,000; discussed in section 5-1-1). Figure 4-17 shows a similar pattern of distribution of landslides produced from the aerial photographs and both the spectral change vector analysis and NDVI change images, which use the multitemporal Landsat TM data. It indicates the high potential of multitemporal Landsat TM data for the identification of landslides. It is, however, impractical to expect exact spatial agreement between these two maps. In this kind of analysis errors are introduced at various stages of the analysis. For example, they are introduced during the preparation of the landslide distribution map from the aerial photographs (also see section 5-5-3), digitization of landslides, transformation of landslide distribution map, and during the rectification of the image from the topographic map. Though it was tried to minimize such errors by taking a lot of precautions, the existence of error can not be ruled out. In addition, landslides in the study area are small in size and 40 percent of them are of single pixel size (30 m x 30 m) limiting the exact spatial agreement between the two maps.

However, it was necessary to quantitatively evaluate the potential of multitemporal Landsat TM data (spectral change vector analysis) for the identification of landslides as well as the sediment deposition area. For this purpose, instead of using all the landslides from the landslide distribution map produced from the aerial photographs, only large landslides (about 100 m wide) plotted from the aerial photographs and also confirmed in the field through the GPS survey were included for the accuracy assessment. The error matrix was generated (see Table 4-14), which consisted of two classes in the change category and one class in the no change category. The reference data used to generate the error matrix then consisted of 388 landslide pixels, and 688 sediment deposited pixels as two classes of change categories, and 1,468 pixels of no change category. The error matrix analysis is carried out here only for change image produced from spectral change vector analysis because the landslide

identification accuracy from NDVI taking into account only the landslide pixels is already shown in Table 4-12 (for explanation see section 4-1-3.2). The pixels in the change image produced from spectral change vector analysis were classified into landslide pixel and sediment deposition pixel based on the pixel's location on the slope gradient map as discussed in section 4-6-2.

Then the modified error matrix (see Table 4-14) shows the overall accuracy and Khat accuracy of 85.6 percent and 74.5 percent, respectively. The accuracy is higher for detecting the sediment deposition class than it is for detecting landslides. The producer's and user's accuracies for sediment deposition class are 80.9 percent and 90.3 percent. The producer's and user's accuracy for landslide class are 57 percent and 74 percent, respectively.

Though the accuracy for detecting landslide was comparatively lower compared with sediment deposition, I judge it to be a very acceptable accuracy. If multitemporal Landsat TM data can provide accuracy of this level it should be considered to have great potential for detecting landslides, because such accuracy has a great value during early assessment.

Another issue was to determine whether or not such a map could be used for the assessment of the landslide hazard. The mapping of landslide distribution is essential in many landslide hazard assessment techniques for the evaluation of site characteristics of existing landslides or land unit associated with landslides. Basically two kinds of unit, a grid-cell unit or catchment/slope-section unit can be used for the assessment of the landslide hazard. The selection of analysis unit in the hazard assessment should be determined by the kinds of data and intended application of its results. The grid cell unit has an advantage over catchment/slope-section unit in providing a detailed hazard map because the relationship between landslide and non-landslide group can be evaluated at the location of the phenomena themselves. The aggregation of data in unit causes a generalization of the input variables in the case of catchment/slope-section unit, which may result in a hazard map that is comparatively generalized. Carrara *et al.* (1991) prefers the use of catchment/slope-section unit in the landslide hazard assessment to minimize the error introduced due to inaccuracy in the landslide distribution map. When the landslide bodies are aggregated at catchment /slope section level, the error is greatly reduced; for example in the case of Carrara *et*

al., (1992) it decreases from 62 percent to 21 percent. When using a grid-cell unit, it should be noted that it is very important to locate landslides correctly.

Since in this study the landslide distribution map produced from the analysis of multitemporal data has comparatively low accuracies, such a map may have limited use in the small grid-cell based hazard assessment. However, the hazard assessments, which use the unit of the analysis as a catchment/slope-section section, may take advantage of such map.

The possible application of the landslide distribution data produced from the multitemporal satellite data in the landslide hazard assessment based on catchment unit was evaluated. The procedure for creating such a catchment map in GIS using DEM is described in Figure 4-18 and Figure 4-19. The process includes the removal of sinks (pits) from the DEM and the calculation of a drainage direction matrix, which is followed by creation of an accumulated area matrix. In the accumulated area matrix layer, each pixel represents the number of pixels that drains into that pixel. A threshold value is then set and a small catchment area is created. It is a sort of semi-automatic process. In this manner, the Kulekhani watershed was divided into 637 catchment units.

These 637 small catchment units were then divided into the landslide catchment units and non-landslide catchment units by overlaying that with landslide distribution map produced from the aerial photographs. Catchment area consisting of landslide(s) was classified as landslide catchment, and without landslide(s) as non-landslide catchment. It shows 263 landslide catchment and 374 non-landslide catchment. Figure 4-20 shows the landslide distribution map produced from the spectral change vector analysis and NDVI using multitemporal Landsat TM data on the top of landslide and non-landslide catchment maps. It shows that more than 80 percent of the landslide catchment units consists of change pixels, i.e. landslides identified using multitemporal Landsat TM data. However, in terms of the total number of pixels, only about 60 percent of the pixels are located on the landslide catchments and 40 percent falls on the non-landslide catchments. It indicates that these change pixels do not contain only landslides but also changes due to other factors as well. In this case, a large number of such pixels were found in the cultivated area, which may have gone changes other than landsliding. The change pixels in the cultivated area basically were presence or absence of crops in two dates. Classifying the change pixels as landslides

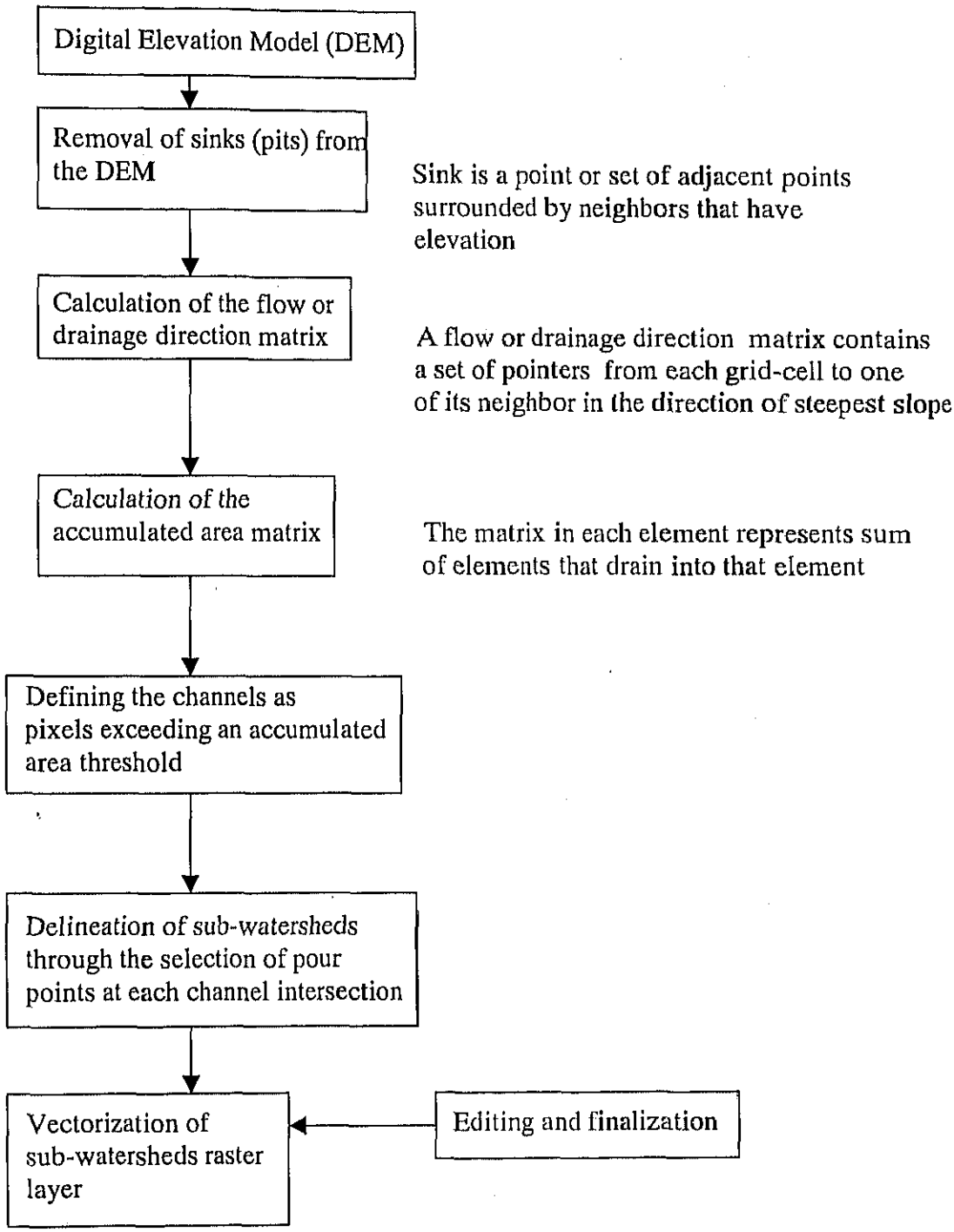

Figure 4-18 Different steps in the processes of creating catchment units using the DEM.

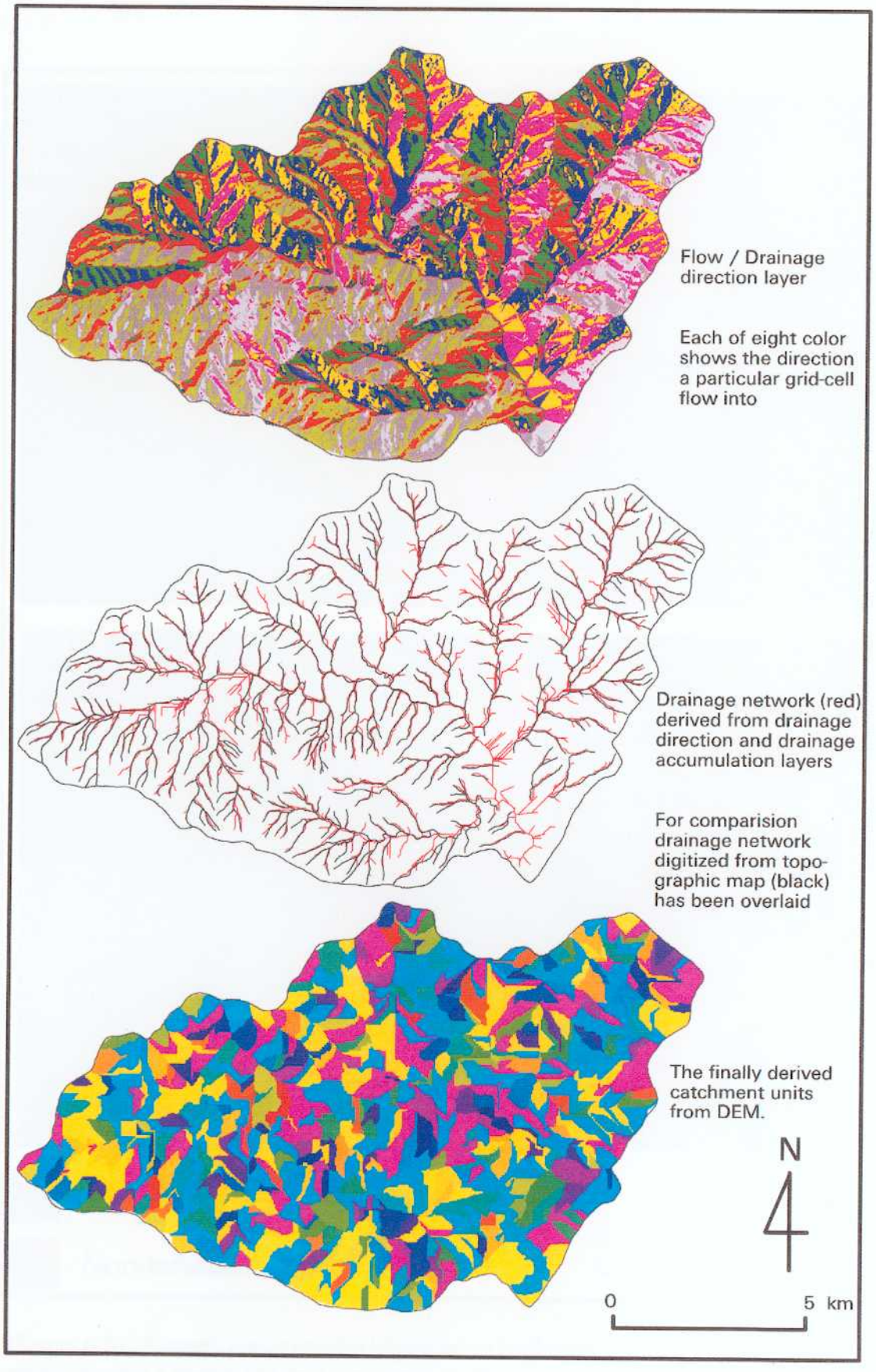

Figure 4-19 Schematic illustration of different steps in the processes of creating catchment units using the DEM.

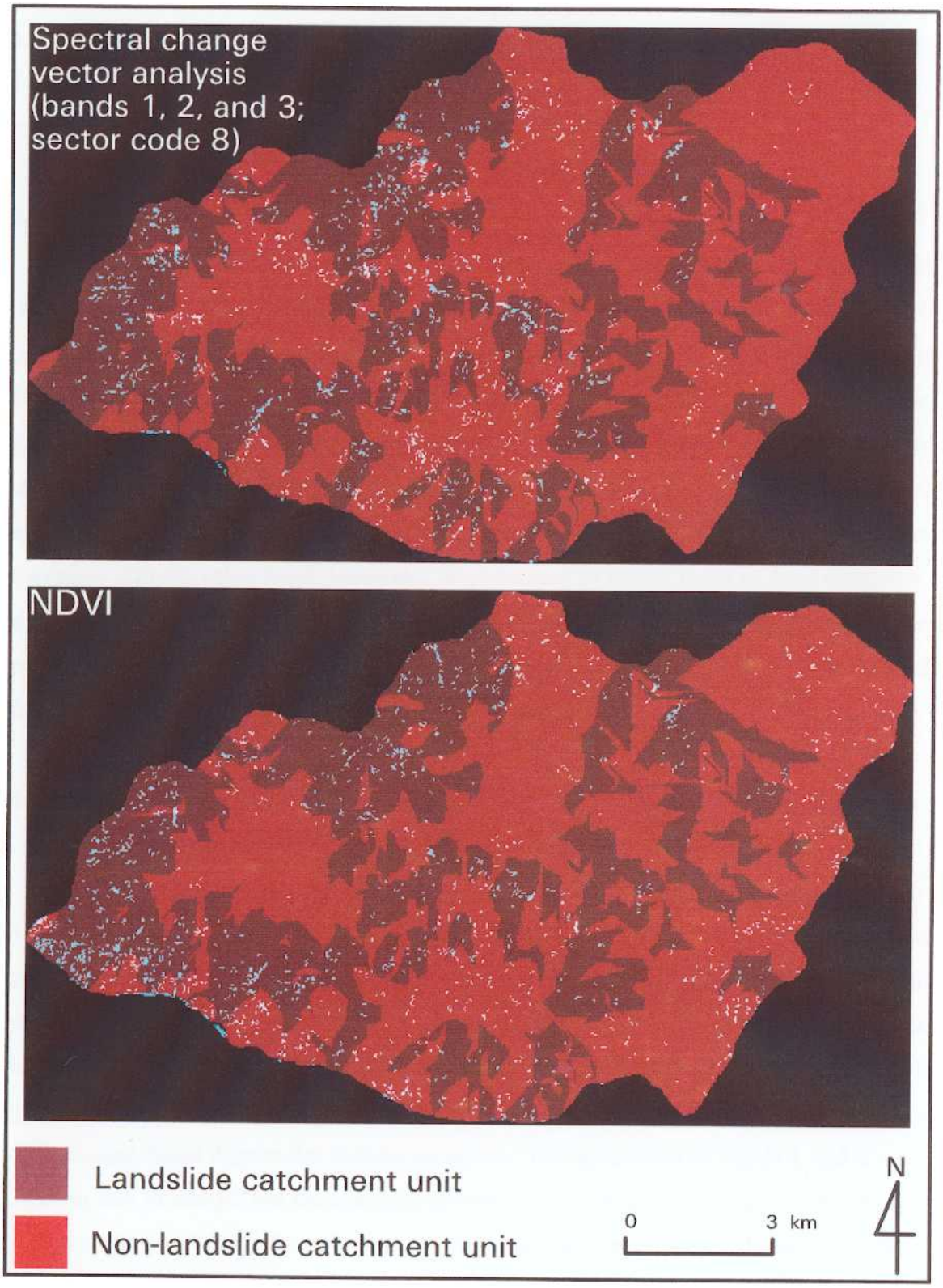

Figure 4-20 Change pixels (white) identified as landslides from the analysis of multitemporal Landsat TM data are shown on the top of landslide and non landslide catchment units identified from landslides interpreted from aerial photographs.

was hence a more difficult task than detecting the change. Though most of the landslides were included in the total change pixels, it was difficult to extract (classify) only landslides from them.

4-3 DISCUSSIONS

The use of multitemporal Landsat TM accomplished very high accuracies (overall accuracy of 88.3 percent and Khat 75.4) for the identification of areas affected by landslides. The accuracies were greatly influenced when different bands and different change detection methods were employed. The accuracies were high for the detection of sediment deposition areas than for just landsliding phenomena. All the sediment depositions occurred in the same type of land use/cover (alluvial fan or river terraces) and their spatial sizes were larger, and this might be the reason for its higher accuracy. On the other hand, landslides were located in all the types of land use/cover, and the detection of changes due to landsliding in all kinds of land use/cover seem to be complex to be detected by a single change detection method. In addition, small size of the landslides may have affected the accuracy assessment.

4-3-1 Potential of Different Bands of TM Data for the Identification of Landslide Affected Areas

Among the seven bands of TM data, three visible bands were found effective in detecting areas affected by landsliding. Though the band 7 also showed the similar characteristics as visible bands, it did not perform well. Bands 4 and 5 showed mixed responses to different kinds of changes associated with landsliding depending on the land use/cover type prior to landsliding. Among the four bands (band 1: blue, band 2: green, band 3: red, and band 7: mid infrared) employed for the spectral image differencing, band 2 gave the highest accuracy. The accuracies of bands 1 and 3 were close to that of band 2 but the accuracy of band 7 was comparatively poor. It indicates that though band 2 performed best in this case, all three visible bands have high potential for detecting changes associated with landsliding. Miller *et al.* (1983) and Patel *et al.* (1985) had found higher reflectance for band 3 (red) for muddy water, which was useful for the estimation of rice yield. Yamagata and Akiyama (1988) had adopted the same hypothesis of band 3 to estimate the paddy damaged by flooding. They used

multitemporal Landsat data in their analysis. However, they did not compare band 3 with band 1 and band 2. In this study, however, the deposited sediments were larger than clay in particle size and mostly varied from sand to boulder and consequently it showed that band 2 is better than band 3. Macleod and Congalton (1998) found the results of band 1 and band 4 better when they employed four bands (band 1, band 2 band 3, and band 4) for the monitoring of eelgrass (flowering plant that is found in shallow sea water) using multitemporal Landsat TM data. It indicates that depending on the type of change we aim to detect, different bands may behave differently.

Band 2 performed best for the detection of landslide affected areas and bands 1 and 2 also showed higher accuracies. Though it is possible that the exactly same result may not be encountered if it is applied to a different ecosystem area, affected by a different intensity of disturbance, the result should not be significantly different. Since the research of this kind is rather limited, the results of this study will serve a guide for using different bands of TM data for the analysis of landslide affected areas.

4-3-2 Evaluation of Change Detection Techniques

An analysis of the different change detection techniques indicates that different methods of change detection produce different maps of areas affected by landslides. The type of sediments and the type of the land cover prior to the disturbances influenced the change detection techniques.

Among five change detection techniques employed, three of them (TM bands, vegetation index, and tasseled cap transformation) were image differencing, in which an image (enhanced or without enhanced) of one date was subtracted from the image of another date. Image differencing is a relatively simple method to understand. Spectral change vector and principal component analyses were the other two techniques employed. Spectral change vector analysis (using bands 1, 2 and 3) performed best to detect the landslide affected areas with the overall and Khat accuracies of 88.3 percent and 75.4 percent followed by band 2 image differencing and principal component analysis. NDVI performed the best among the four algorithms that were especially employed to determine the vegetation responses to landsliding.

Michalek *et al.* (1993) found spectral change vector analysis as an effective technique to monitor coastal marine environments, though they did not quantitatively

assess the accuracy. A study conducted by Michener and Houhoulis (1997) for the detection of vegetation changes associated with flooding in forested ecosystem of southwest Georgia, USA, showed NDVI image differencing as the most effective technique for discriminating vegetation responses to flooding, followed by principal component analysis. They had compared five different techniques of change detection. Muchoney and Haack (1994) carried out a study on forest defoliation using multitemporal SPOT (Haute resolution visible; HRV) XS data. They found the principal component analysis and the image differencing as having potential for achieving reliable mapping of defoliation, among the five different techniques employed for the study. Yamagata and Akiyama (1988) reported good results of the principal component analysis for flood damage analysis though they did not quantitatively evaluate the method.

The results indicate that the change detection techniques should be selected depending on the type of change we want to extract. Hence, it is essential to explore and compare a variety of change detection techniques for their applicability to a particular problem. The results of this study show how the selection of change detection analysis should be decided for similar studies to be carried out in the future. When a single homogenous land use/cover experience the disturbances, it might be easy to perform the change detection methods and compare them. When analysis of landslide affected areas is carried out in a watershed, which consists of different land use/cover, the problem becomes complex because of different responses of bands with respect to land use/cover. It is possible that different bands or different techniques may be effective for different types of change, or change in the different types of land use/cover. Some authors have combined the best threshold images for different bands and compared that to the reference data. For example, Macleod and Congalton (1998) combined threshold change images of bands 1, 2, 3 and 4 to produce bands 1, 2, and 4 image; bands 1 and 4 image; and bands 1, 3, and 4 image. However, this kind of analysis again makes the problem more complex and such analysis was avoided in this study.

Another critical part of all the detection techniques is the determination of threshold value. The method of selection of threshold value applied in this study is the best method. The accuracy assessment may be sometimes critical because it is often based on the minimum samples because in practice there is always a compromise with

the sampling size of reference data. In this study about 3,000 pixels were used as reference data out of a total of about 140,000 pixels. This is quite sufficient for this kind of analysis. Previous similar studies also used similar sample size. Hence, when working with remotely sensed data ground truth is the most important aspect. The reference data should be error free. This study first determined the reference data in large-scale photographs, which were then plotted onto the topographic map using a stereo zoom transferscope. The topographic map was then taken into the field and a GPS survey was carried out for confirmation. Since the accuracy assessment is a relative one, it is expected that any error introduced in the reference data would have equal impact in the accuracy assessment of the techniques employed.

Classification of the change pixels is another critical aspect. This study uses a slope gradient map produced from the DEM for the classification of change pixels. The landslide and sediment deposition pixels were classified according to their position in the slope gradient map. The method is very practical in this kind of analysis, because classifications of change pixels are often a difficult task. However, in many cases DEM may not be available hindering such an efficient classification system. An analysis of two images independently for the classification purpose is not an impossible task. However, the extraction of classes from a single image such as sediment deposition or landslide is greatly limited depending on the background contrast.

4-3-3 Identification of Landslides from the Multitemporal Landsat TM Data

The multitemporal Landsat TM data proved to be very promising in the detection of landslide affected areas, especially if the results are necessary for an early assessment. The sediment deposition area was more correctly determined than was possible for landslides. In the early assessment, this level of information is very adequate. In 1993 disaster the roads to the Kulekhani watershed had been washed away and for about a month one could reach there only on foot. The complete assessment of the disaster was not available even after many months of the disaster. In Nepal, it is not usual to have aerial photographs just after the disaster because of economic constrain. It is mostly influenced by external funds from the donor agency. Since it is often a long process, aerial photographs can not be taken immediately after an event. For example, in this case aerial photographs were taken 8 months after the disaster. The availability of

continuous images from satellite is hence very promising for the early assessment of the disaster in this part of the world. The cloud influences this kind of satellite data, and many times it is difficult to find cloud free data. However, the choice of many kinds of data available at present (such as Landsat TM, SPOT, IRS) and many more satellite plans of the future indicate that problems relating to the unavailability of data will gradually diminish. The theory behind the detection would be the same irrespective of which data is used, as long as the band has similar characteristics.

One of the important aspects of this study is the use of multitemporal data for the extraction of landsliding. In previous studies (e.g., Aniya *et al.*, 1985b; Sakai *et al.*, 1985; Rengers *et al.*, 1992; Mantovani *et al.*, 1996) a significant success in identifying landslides could not be achieved because all those studies were based on the analysis of a single image. In those studies, the background contrast and the spatial resolution of the satellite data might have limited the identification. Landsliding is not a gradual process such as land use change. Landslides occur due to some certain events such as heavy rainfall, and this characteristic is advantageous for detection analysis. When data taken prior-to and after such an event are analyzed, landslides will be detected with very high confidence. The producer's and user's accuracy for landslide identification in this study was 56.7 percent and 73.6 percent respectively. This accuracy should be considered to be rational considering the different problems associated with accuracy assessment. The landslides in the study area are small in size and 40 percent of them are of single pixel size. When the size of the landslide is small like this it is often difficult to evaluate the result precisely because of the errors that are introduced at various stages of the analysis.

When the pixels identified as landslides by analyzing multitemporal Landsat data were compared with the landslide and non-landslide catchment units, derived from the DEM and landslides interpreted from aerial photographs, the agreement was remarkably high. The landslide and non-landslide catchment units interpreted from aerial photographs and multitemporal Landsat TM data agreed to 80 percent. It indicates that the landslide distribution data extracted from the multitemporal Landsat TM data can be used for the landslide hazard assessment processes, which use catchment area as an analysis unit. It should be however kept in the mind that in terms of total number of pixels, about 40 percent of the pixels were located on the non landslide catchments. It

indicates that these change pixels do not contain only landslides (despite the fact that many classification systems were applied) but changes due to other factors as well. In this study, large number of such pixels were found in cultivated area, which have undergone changes other than landsliding such as presence or absence of crops. This kind of problem may be avoided if the pre and post disaster images can be found with a relatively short time span of less than 1-2 months. In this case such images were not available. With more satellite data to come in the future it is possible that such data would be available.

The landslide identification from multitemporal Landsat TM data proved to be effective for the analysis based on the catchment units; however, it is not suitable for the grid-cell based hazard assessment. For this reason, the methods of landslide hazard assessment discussed in the next section use the landslide distribution map produced from large scale aerial photographs. The grid cell unit approach was employed considering the availability of substantial accurate landslide distribution map. The analysis in the grid cell unit provides more detailed map. Different issues of using grid-cell based landslide hazard assessment are also covered. The next section also discusses about landslide hazard mapping and the evaluation of landslide hazard maps. The methods described for landslide hazard assessment, mapping and evaluation of hazard maps in the next section can be used in a similar manner, if the landslide hazard assessment is carried out based on the catchment unit.